Oscillations in the bistable regime of neuronal networks

Alex Roxin

Computational Neuroscience Group, Centre de Recerca Matemàtica, Campus de Bellaterra, Edifici C, Bellaterra 08193, Spain

Albert Compte

*Theoretical Neurobiology of Cortical Circuits, Institut d'Investigacions Biomèdiques August Pi i Sunyer (IDIBAPS),
Carrer Rosselló 149, Barcelona 08036, Spain*

Bistability between attracting fixed points in neuronal networks has been hypothesized to underlie persistent activity observed in several cortical areas during working memory tasks. In network models this kind of bistability arises due to strong recurrent excitation, sufficient to generate a state of high activity created in a saddle-node (SN) bifurcation. On the other hand, canonical network models of excitatory and inhibitory neurons (E-I networks) robustly produce oscillatory states via a Hopf (H) bifurcation due to the E-I loop. This mechanism for generating oscillations has been invoked to explain the emergence of brain rhythms in the β to γ bands. Although both bistability and oscillatory activity have been intensively studied in network models, there has not been much focus on the coincidence of the two. Here we show that when oscillations emerge in E-I networks in the bistable regime, their phenomenology can be explained to a large extent by considering coincident SN and H bifurcations, known as a codimension two Takens-Bogdanov bifurcation. In particular, we find that such oscillations are not composed of a stable limit cycle, but rather are due to noise-driven oscillatory fluctuations. Furthermore, oscillations in the bistable regime can, in principle, have arbitrarily low frequency.

I. INTRODUCTION

The simplest canonical cortical circuit consists of a single population of excitatory neurons and a single population of inhibitory neurons (E-I network). Models of E-I networks robustly exhibit nontrivial computational and dynamical properties due to the occurrence of transitions in the qualitative behavior of the system, called bifurcations. In particular, for sufficiently strong excitation a region of bistability between a low-activity and a high-activity state can arise via a pair of saddle-node (SN) bifurcations [1–3]. E-I networks also readily generate oscillations via a Hopf (H) bifurcation when excitation is sufficiently strong and fast [4,5]. The frequency of these oscillations, within the γ range (30–100 Hz), is predominantly set by the E-I loop, and in particular by the ratio of excitatory to inhibitory synaptic time constants. This mechanism contrasts with the I-I loop, which underlies the generation of fast oscillations ($>$100 Hz), the frequency of which is set by the inhibitory synaptic delay [5,6]. Both mechanisms are present in an E-I network and contribute to the population frequency with the E-I loop dominating when recurrent excitation is strong. Theoretical work therefore suggests that when recurrent excitation is strong enough it ought to be possible to obtain robust oscillations in the bistable regime in E-I networks via the E-I loop alone.

Experimentally, in both humans and nonhuman primates oscillations in several different frequency bands have been observed to correlate with memory demands during working memory tasks, including θ (4–8 Hz) [7–10], α to β (8–30 Hz) [11–13], and γ (20–100 Hz) [14–16]. The functional role of oscillations during working memory tasks is not known, although it has been hypothesized to orchestrate the co-ordinated computation of different brain regions through synchronization [17]. Besides doubts regarding the functional role of oscillations during working memory tasks, it is also

unknown what the physiological mechanisms which generate them are. The most parsimonious mechanism would be the E-I loop itself, without recourse to additional neuronal subtypes, network structure, or single-cell properties.

In this paper, we explore the phenomenology of oscillations in E-I networks in the bistable regime. We show that oscillations are qualitatively distinct from those which appear in the nonbistable regime (we can say "linear regime"). Specifically, the presence of SN bifurcations, which generate the bistable behavior, impose certain topological constraints on the oscillatory dynamics which have two main consequences: (1) Oscillations are subcritical and there is no stable limit cycle over a large parameter range; (2) oscillations can have arbitrarily low frequency. The first consequence means that oscillations are generically damped in the bistable regime. Hence, oscillations are only observable as a transient response to time-varying input or as a sustained resonant response in the presence of stationary fluctuations (for example, an external noise source). The second consequence indicates that the E-I loop alone can, in principle, account for oscillations throughout the δ to γ range (roughly 1–100 Hz) in the bistable regime.

II. FIRING RATE MODEL

In this paper we consider a canonical cortical circuit composed of recurrently coupled excitatory (E) and inhibitory (I) neurons. In particular we study the phenomenology of oscillations which arise through the E-I loop in the bistable regime.

We first analyze a reduced model of firing-rate equations for a network of E and I neurons. Specifically, we consider a single continuous variable to represent the mean activity in each of the two neuronal populations [1,2], resulting in a system of two coupled differential equations. In general, it is

not possible to derive such mean-field models rigorously from a network model of spiking neurons, although see [18–20]. The benefit of the reduced system is that it is amenable to analysis. Finally, we compare the results from the reduced system to some analysis and numerical simulations of a network of leaky integrate-and-fire neurons.

The firing-rate equations we study are

$$\tau_e \dot{r}_e = -r_e + \phi_e(I_e), \quad \tau_i \dot{r}_i = -r_i + \phi_i(I_i), \quad (1)$$

where

$$
\begin{aligned}
I_e(t) &= J_{ee}s_{ee}(t) - J_{ei}s_{ei}(t) + I_{ext,e}(t), \\
I_i(t) &= J_{ie}s_{ie}(t) - J_{ii}s_{ii}(t) + I_{ext,i}(t),
\end{aligned}
\quad (2)
$$

where $J_{ab}s_{ab}(t)$ represents the population-averaged value of the synaptic input from a neuron in population b to a neuron in population a. The parameter J_{ab} is the mean synaptic strength, while the variable $s_{ab}(t)$ is the level of activation of the corresponding synapses. If we ignore the synaptic time course, which is equivalent to assuming that postsynaptic currents (PSCs) are fast compared to the time constants of the firing rates, then the mean synaptic activation is identically equal to the mean firing rate of the presynaptic population with a delay, i.e., $s_{ab}(t) = r_b(t - D_{ab})$, where D_{ab} is the synaptic delay from population b to population a.

Alternatively, we can include the synaptic time course by solving the equations

$$
\begin{aligned}
\tau_{d,b}\dot{s}_{ab} &= -s_{ab} + x_{ab}, \\
\tau_{r,b}\dot{x}_{ab} &= -x_{ab} + r_b(t - D_{ab}).
\end{aligned}
\quad (3)
$$

Here x is an intermediate synaptic variable which leads to a difference-of-exponential time course, where $\tau_{d,a}$ and $\tau_{r,a}$ are the rise and decay time constants of the synapses of type $a \in \{e,i\}$.

Equations (1)–(3) are a heuristic, mean field model of the activity in a cortical microcircuit. Under very generic constraints on the transfer functions ϕ_e and ϕ_i this model can generate oscillations and exhibit bistability between a low-activity and a high-activity state. Both of these dynamical regimes are of relevance for real brain circuits, and for this reason the equations have been extensively studied. Nonetheless, less attention has been paid to the regime in which both types of behavior coincide, namely when an oscillatory instability occurs in the bistable regime.

A. Steady state solutions and their stability

The steady state fixed points of the model are found by setting the time derivatives in Eqs. (1)–(3) equal to zero. The resulting system of (in general) transcendental equations is not usually analytically tractable. Nonetheless, the fixed-point space is reducible to two dimensions, in r_e and r_i, allowing for a simple geometric analysis. The resulting number of fixed points clearly depends on the shape of the transfer functions ϕ_e and ϕ_i. Luckily, these are strongly constrained by having to correspond to the mean field transfer functions for networks of spiking neurons. This implies that they are monotonically increasing with a concave upwards regime at low rates and a concave downwards regime at high rates

[21–23]. These two regimes correspond to the fluctuation-driven, subthreshold regime of neuronal spiking and the mean-driven, suprathreshold regime of neuronal spiking, respectively. We discuss this more in-depth later on in the section on spiking networks.

With these constraints the model Eqs. (1)–(3) generically admit either a single, stable fixed point or three fixed points, two of which are stable and correspond to a low-rate and a high-rate state. It is in this second regime that the model exhibits bistable behavior. We write the fixed-point solutions (r_{e0}, r_{i0}) to Eqs. (1)–(3) as

$$
\begin{aligned}
r_{a0} &= \phi_a(I_{a0}), \\
I_{a0} &= J_{ae}r_{e0} - J_{ai}r_{i0} + I_{ext,a},
\end{aligned}
\quad (4)
$$

where $a \in \{e,i\}$.

Whether there is one fixed point or there are three, the stability of each one is determined by slightly perturbing the fixed-point solution and studying the linearized dynamics. This leads to the eigenvalue equation

$$[1 - A_{ee}(\lambda)][1 + A_{ii}(\lambda)] + A_{ei}(\lambda)A_{ie}(\lambda) = 0, \quad (5)$$

where $A_{ab}(\lambda) = J_{ab}R_a(\lambda)S_{ab}(\lambda)$ depends on the neuronal response function of population $aR_a(\lambda)$ and the synaptic response function $S_{ab}(\lambda)$. These functions are

$$
\begin{aligned}
R_a(\lambda) &= \frac{\phi_a'(I_{a0})}{(1 + \tau_a \lambda)}, \\
S_{ab}(\lambda) &= \frac{e^{-D_{ab}\lambda}}{(1 + \tau_{d,b}\lambda)(1 + \tau_{r,b}\lambda)}.
\end{aligned}
\quad (6)
$$

B. Rate equations without synaptic dynamics

In the simplest case we ignore both the synaptic dynamics and the synaptic delay. In this case, Eq. (5) gives a condition for a steady instability (saddle-node bifurcation),

$$J_{ee}\phi_e' > 1 + \frac{J_{ei}J_{ie}\phi_i'\phi_e'}{1 + J_{ii}\phi_i'}, \quad (7)$$

which means that when the strength of recurrent excitatory synapses (J_{ee}) times the gain in the response of the population of excitatory cells (ϕ_e') reaches a critical value (the right-hand side of the equation), there is a jump in the network activity. Two such saddle-node bifurcations leading to a switch from low-rate to high-rate activity, and vice-versa, encapsulate the bistable regime. Note that the slope of the transfer function (gain) is evaluated at the fixed point [$\phi_e' = \phi_e'(I_{e0})$].

The condition for an oscillatory instability is the following:

$$J_{ee}\phi_e' > 1 + \frac{\tau_e}{\tau_i}(1 + J_{ii}\phi_i'). \quad (8)$$

Therefore, the appearance of oscillations depends crucially on the value of the ratio of the excitatory and inhibitory time constants.

Both of these instabilities can occur for the same parameter values. In fact, it is clear that an oscillatory instability can be made to occur in the model near a saddle-node bifurcation by appropriately adjusting the time constants, for example. Characterizing the resulting dynamical behavior in the vicinity of these two instabilities is the major goal of this paper.
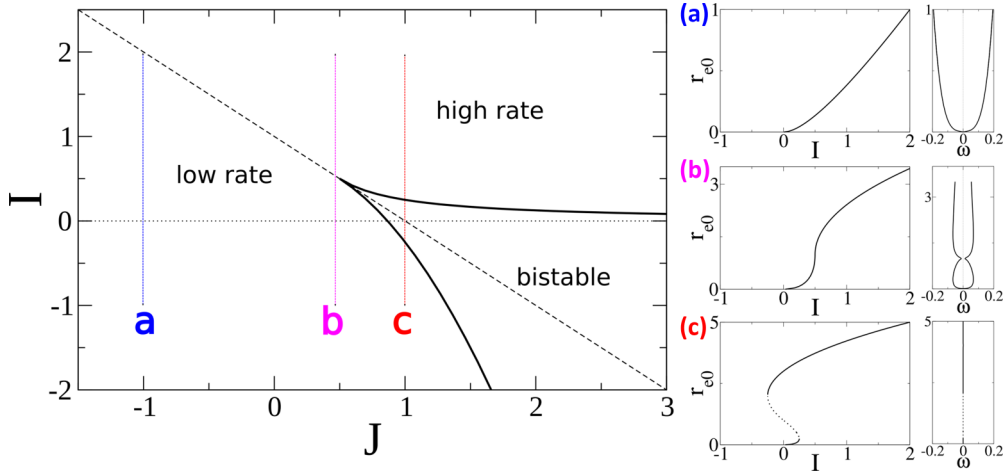
FIG. 1. The phase diagram for the firing-rate model Eqs. (1). The transfer function for the excitatory population is given by Eq. (10), while it is linear-threshold for the inhibitory population. The solid lines are the saddle-node bifurcation lines, which meet as a cusp at $(I,J) = (1/2,1/2)$. To the left of this point there is only a single fixed point, while to the right there are three. The low-rate solution reaches zero at $I = 0$ (dotted line), while the low-rate and high-rate solutions meet along the diagonal $I = 1 - J$ (dashed line). The feedforward inhibition $\beta = 1$, while the time constant ratio $\tau = 2$. There are no oscillatory instabilities, so the saddle-node lines provide a complete description of the possible bifurcations. (a)–(c) Sample bifurcation diagrams taken along the cuts shown in the phase diagram. The right panel is the frequency of the most unstable eigenvector. Stable branches are solid lines and unstable ones are dotted. Here $\tau_e = \tau_i = 10$, $J_{ii} = 1$, $J_{ie} = J_{ei} = \sqrt{2}$.

C. An analytically tractable example

It is helpful to make a concrete choice for the transfer functions ϕ_e and ϕ_i so that a systematic and exhaustive analysis can be done without resort to numerical simulations. For the inhibitory population we choose a simple threshold linear function, i.e., $\phi_i(I) = I$ as long as $I > 0$; otherwise, it is zero. In this case the fixed-point equations can be reduced to a single dimension and expressed only as a function of r_{e0},

$$r_{e0} = \phi_e(Jr_{e0} + I), \qquad (9)$$

where $J = J_{ee} - \frac{J_{ei}J_{ie}}{1+J_{ii}}$ and $I = I_{e0} - \frac{J_{ei}I_{i0}}{1+J_{ii}}$. The fixed-point value of the inhibitory rate is just $r_{i0} = (J_{ie}r_{e0} + I_{i0})/(1 + J_{ii})$.

Here we take the following shape for the excitatory transfer function:

$$\phi_e(x) = \begin{cases} 0, & \text{if } x < 0, \\ x^2, & \text{if } 0 \leqslant x \leqslant 1, \\ 2\sqrt{x - 3/4}, & \text{if } x > 1. \end{cases} \qquad (10)$$

This choice captures the fluctuation-driven regime (quadratic nonlinearity) and the mean-driven regime (square-root nonlinearity) in the simplest possible way.

With this choice of transfer function we can solve the fixed-point equation, Eq. (9), analytically. Figure 1 shows the resulting phase diagram of the fixed-point solutions. For $J < 1/2$ there is only a single fixed point, while for $J > 1/2$ there are three. This region of bistability is delineated by the two saddle-node lines given by

$$I_{SN}^L = \frac{1}{4J}, \quad I_{SN}^H = \frac{3}{4} - J^2, \qquad (11)$$

where the superscripts refer to a bifurcation of the low-rate (L) or the high-rate (H) state.

In the phase diagram the two firing regimes, which we call low-rate and high-rate and which correspond to

the quadratic and square-root nonlinearities of the transfer function, Eq. (10), respectively, meet along the line $I = 1 - J$. This is shown as a dashed line in Fig. 1. Below $I = 0$ (dotted line in Fig. 1) the excitatory firing rate r_{e0} is equal to zero.

The saddle-node lines [Eqs. (11)] can be derived directly from Eq. (9), but they are also equivalent to the stability condition Eq. (7). The other stability condition, Eq. (8), can be reduced to the conditions

$$I_{Hopf}^L = \frac{1}{4J}\left[1 - \frac{(\beta - \tau J)^2}{(\beta + J)^2}\right],$$
$$I_{Hopf}^H = \frac{3}{4} - J^2 + \frac{(\beta - \tau J)^2}{(1 + \tau)^2}, \qquad (12)$$

where the parameter $\beta = J_{ei}J_{ie}/(1 + J_{ii})$ is the feedforward inhibition to the excitatory population. The parameter $\tau = (\tau_e/\tau_i)(1 + J_{ii})$ is an effective time constant which is large if excitation is much slower than inhibition and small if inhibition is slower than excitation.

The Hopf bifurcation lines Eqs. (12) exist only if $\tau < 2\beta$. In the phase diagram Fig. 1 we have chosen $\tau = 2$ and $\beta = 1$, so there are no Hopf bifurcations, and the saddle-node lines give the full picture. This does not mean that there are no oscillatory dynamics, however. Panels (a), (b), and (c) show bifurcation diagrams along the cuts indicated in the phase diagram. In the bifurcation diagrams stable fixed points are drawn as solid lines and unstable ones are dotted lines. To the right of each bifurcation diagram is the frequency of oscillation, i.e., the imaginary part of the eigenvalue of the most unstable eigenvector. In panels (a) and (b), for example, linear perturbations of the fixed-point solution are always stable, but they oscillate. That is, there are damped oscillations. Note that we have taken the parameters in the firing rate equation to be unitless; because they are not derived from first principles, the choice of units is arbitrary. The oscillation frequency in Fig. 1 should therefore be measured relative to the time constants
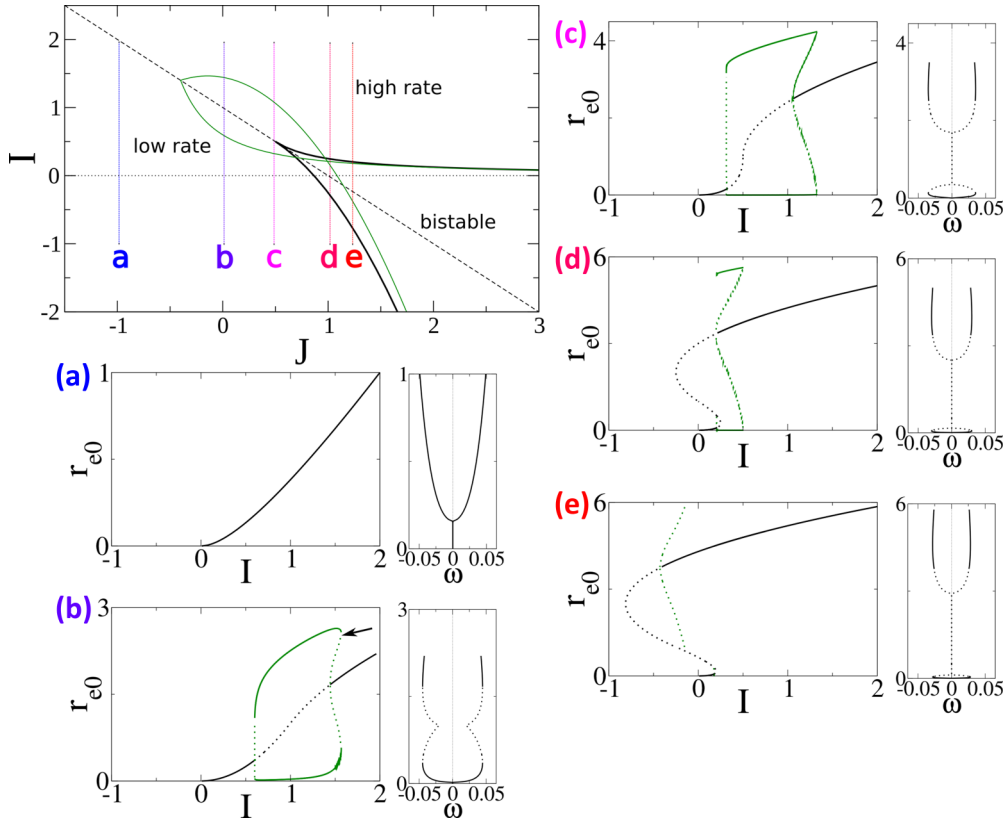
FIG. 2. The phase diagram for the same firing-rate model as in Fig. 1. Here the only change is that $\tau_i = 100$ ($\beta = 1$ as before), which is equivalent to increasing the inhibitory time constant compared to Fig. 1. Because $\tau < 2\beta$, there are now two Hopf-bifurcation lines, shown in green. The saddle-node lines are the same as before. The two Hopf-bifurcation lines meet along the diagonal $I = 1 - J$ at a point which is approximately $(I^*, J^*) = (1/2 + \beta, 1/2 - \beta)$. This approximation is exact in the limit $\tau \to 0$. The frequency of oscillation along these lines increases to the left and reaches a maximum exactly at the point (I^*, J^*). As $\tau \to 2\beta$, the point (I^*, J^*) moves towards $(1/2, 1/2)$ and the maximum frequency goes to zero. (a)–(e) Sample bifurcation diagrams taken along the cuts shown in the phase diagrams. Black lines are fixed points and green lines are limit-cycles. Solid lines are stable solutions and dotted lines [panel (c)] unstable ones. $\tau_i = 100$, all other parameters are as in Fig. 1.

$\tau_e = \tau_i = 10$. For example, if we choose units of milliseconds, then the value $\omega = 0.2$ in Fig. 1 corresponds to about 32 Hz.

For $\tau < 2\beta$, the two Hopf bifurcation lines meet along the diagonal at a point (I^*, J^*). The frequency of the instability along these lines increases for decreasing J and reaches a maximum precisely at this point. The frequency along the lines is

$$\omega = \pm \frac{1}{\tau_e} \sqrt{\frac{\tau(\beta - \tau J)}{(\beta + J)}}, \qquad (13)$$

which has a maximum

$$\omega^* = \pm \frac{1}{\tau_e} \sqrt{\tau(2\beta - \tau)}, \qquad (14)$$

from which is it easy to see that the maximum frequency goes to zero when $\tau = 2\beta$. This occurs at the point $(I^*, J^*) = (1/2, 1/2)$. While the value of this point for the general case of $\tau < 2\beta$ is a complicated formula, it takes a simple form in the limit $\tau \to 0$, namely $\lim_{\tau \to 0}(I^*, J^*) = (1/2 + \beta, 1/2 - \beta)$.

Figure 2 shows the phase diagram when $\beta = 1$ and $\tau = 0.2$. The Hopf bifurcation lines are shown in green. From the limiting case, we expect the point (I^*, J^*) to be just to the right and below $(3/2, -1/2)$, which it is. Example bifurcation

diagrams are shown in panels (a) through (e). Fixed points are the black lines as before, whereas periodic limit cycles are shown as green lines. Solid lines are stable solutions and dotted lines are unstable solutions. Note that the plots of the frequency of oscillation to the right of each bifurcation diagram refer to perturbations of the fixed-point solution, not to the limit cycle if there is one.

If we look at the bifurcation diagrams from (a) to (e) in succession in Fig. 2, we see changes in the nature of the oscillatory solutions. Furthermore, these changes are related to the presence of the saddle-node bifurcations. Let us first consider panels (b) and (c), which lie to the left of the saddle-node lines, in the regime where there is only a single fixed point. In these two panels, there is a subcritical Hopf bifurcation at the critical values of the input I (the green lines in the phase diagram). This means that the limit cycle which grows continuously from the point of instability (as a function of I in the panels) is unstable. At some point it meets and annihilates with a large-amplitude limit cycle which is stable. This so-called "saddle node" of limit-cycles bifurcation is indicated in panel (b) with an arrow.

The nature of the Hopf bifurcation (super- or subcritical) can be determined by carrying out a weakly nonlinear

analysis at the bifurcation point; see the Appendix. The Hopf bifurcation is subcritical if

$$J + \frac{3}{5} \frac{\phi_e'''}{(\phi_e'')^2} \frac{(\beta - \tau J)}{(\beta + J)} > 0. \tag{15}$$

For the low-rate fixed point $\phi_e''' = 0$, which means that limit cycles are supercritical for $J < 0$ and subcritical for $J > 0$. For the high-rate fixed point one can show that the bifurcation is always subcritical.

To the right of the saddle-node lines, in the regime where there are three fixed points, the situation is different. In panel (d) we see that there is a subcritical Hopf bifurcation of the high-rate fixed point, but the resulting large-amplitude limit cycle suddenly vanishes in the middle of the "s-shaped" region, leaving the unstable fixed point to the left without a limit-cycle solution. Figure 3 shows the same bifurcation diagram with a close-up of the low-rate branch. By magnifying we see that there is also a subcritical Hopf bifurcation of the low-rate state, as expected, and that the unstable limit cycle (dotted green line) meets and annihilates with the large-amplitude stable limit cycle. However, this occurs to the right of the leftmost saddle-node bifurcation. This means that the high-rate fixed point in the "bistable" regime (it is not bistable) is an unstable spiral which does not lead to a stable limit cycle.

In this regime the model exhibits an interesting "all-nor-none" response to transient external inputs, similar to the action potential of a neuron. If the steady input is fixed at, for example, $I = 0$ in Figs. 2(d)–3(d), then a small transient increase in input to the excitatory population would just decay away to zero, which is the only stable solution. If, however, the transient input is strong enough to increase the firing rate above the saddle point (middle dotted line in the "s-shaped" region), then the rate will increase beyond the unstable high-rate fixed point and circle back down to zero again. More specifically, there is a separatrix in phase space which separates those inputs which decay to zero monotonically, from those which undergo an excursion. In the case of the simple two-variable model Eqs. (1) without delays, this separatrix is just the stable manifold of the saddle point.

An illustration of this all-or-none effect can be seen in Fig. 4. As the amplitude of the transient input is increased, a threshold is reached, beyond which there is a large excursion, the shape of which is essentially independent of the stimulus strength. The latency of the onset of the excursion does depend on stimulus strength, as with action potentials in neurons. To close the analogy, excitation and inhibition are like Na and K. The conditions for this behavior in the firing-rate model are that the recurrent excitation be strong ($J > 1/2$) and that excitation be sufficiently faster than inhibition $\tau < 2\beta$. Similarly, in order to generate action potentials, the Na conductance must be large, and the Na activation must be fast compared to K.

Finally, another way to get over the separatrix is by inhibiting the inhibitory population, e.g., by reducing its external excitatory drive. This is illustrated in Fig. 5.

Now if we look at Fig. 2(e) we see that the situation has changed yet again. Here there is a subcritical Hopf bifurcation of the high-rate fixed point, as expected, but the unstable limit cycle simply vanishes in the middle of the s-shaped region. If we magnify the low-rate solution, seen in Fig. 3, we see precisely the same type of behavior. In fact, the way the
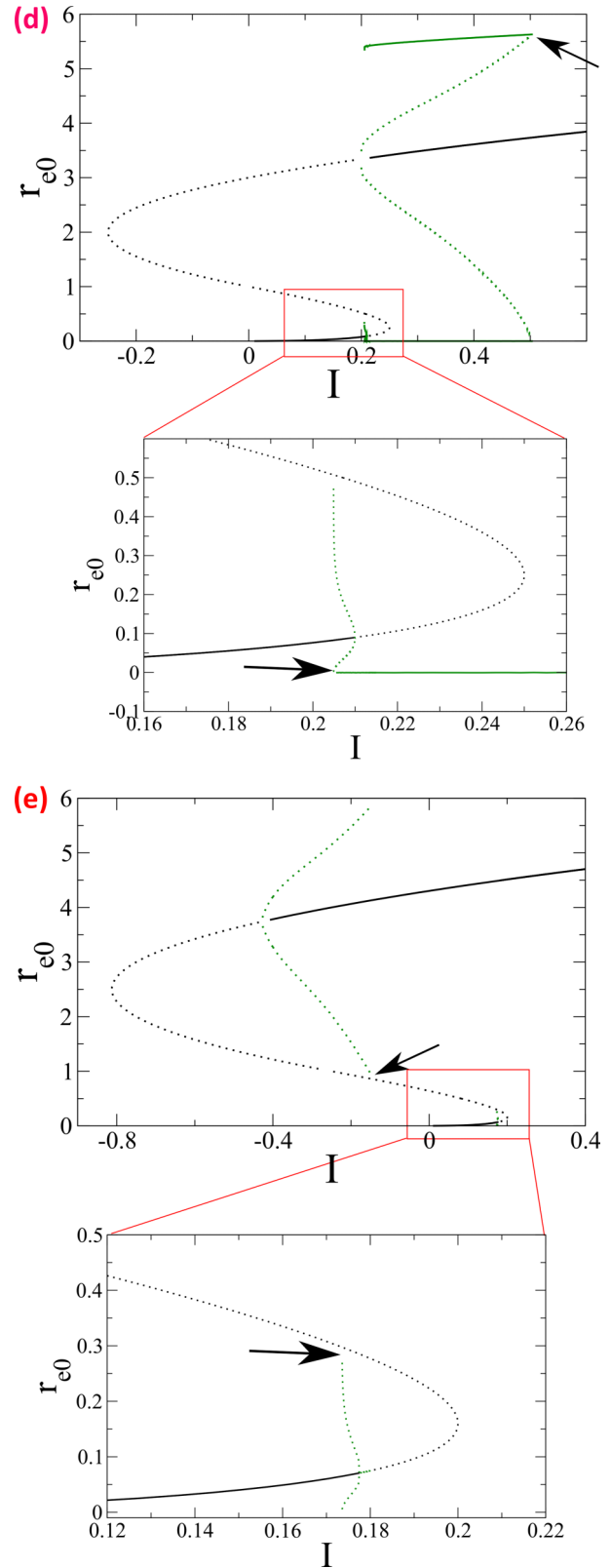

FIG. 3. Panels (d) and (e) from Fig. 2. The close-ups show bifurcations of the low-rate fixed point.

unstable limit cycle disappears is that it touches the saddle point. When it does this, the unstable manifold of the saddle
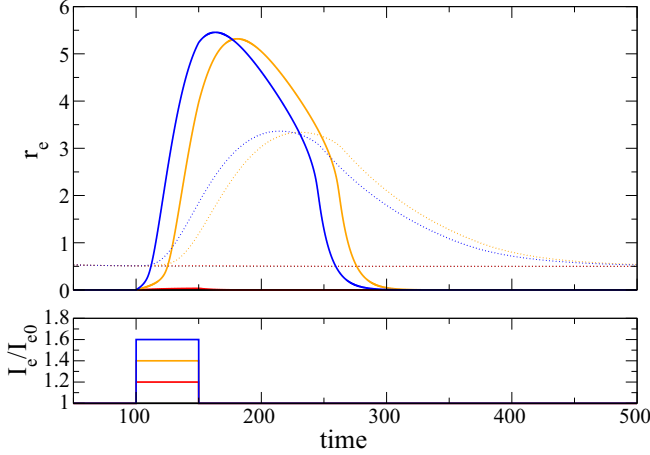
FIG. 4. An all-or-none population spike in the model Eqs. (1). The parameters are $J = 1$, $I = 0$, $\beta = 1$, $\tau = 0.2$, which place the model in the s-shaped regime of Fig. 3(d). The excitatory input is transiently increased between $t = 100$ and $t = 150$. Above a threshold value of the transient input an all-or-none population spike occurs. The inhibitory firing rate is shown as a dotted line.

point circles around and returns to the saddle, i.e., there is a homoclinic bifurcation.

If we increase J even further, we will find no other changes in the bifurcation diagram. There will always be an unstable limit cycle, of both fixed points, and a homoclinic bifurcation, again of both unstable limit cycles. Therefore, there are no stable limit cycles. We can be confident that this is the case, not because we have carried out extensive numerical simulations, but rather because this behavior is predicted from theoretical arguments.

D. The Takens-Bogdanov bifurcation in E-I networks

The reasoning is as follows. If we are interested in oscillations in, or near the bistable regime, then by construction we are near both a saddle-node bifurcation (steady instability) and
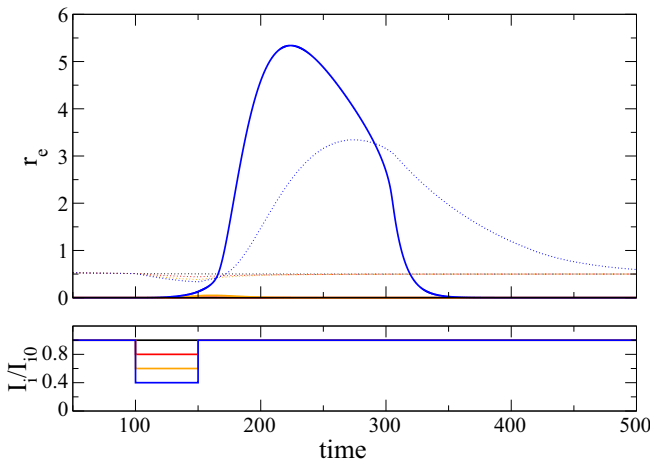

FIG. 5. An all-or-none population spike is generated here by transiently reducing the excitatory drive to the inhibitory population. The parameter values are the same as in Fig. 4

a Hopf bifurcation (oscillatory instability). In our two-variable firing-rate model this means that we are near a set of parameter values for which both eigenvalues are zero; this is known as a Takens-Bogdanov bifurcation. This double-zero eigenvalue problem has been extensively studied for the general case (see [24] for detailed description). Like all local bifurcations, the dynamics near this point are well described by a simplified equation (or set of equations), which are universal. That is, the form of the reduced equations only depends on there being two zero eigenvalues, not on the details of the original equations. The exact parameter values in the reduced equations, however, do depend on the details. In the next section we give a detailed description of this bifurcation for Eqs. (1). The Takens-Bogdanov (TB) bifurcation can exhibit two distinct behaviors depending on the sign of the nonlinear terms in the reduced or amplitude equations. Therefore, in order to determine which case is the relevant one for the firing-rate equations we are studying, we derive the amplitude equations. We provide an overview of the procedure in this section and relegate the detailed calculation to the Appendix.

In the vicinity of the TB bifurcation in Eqs. (1) with instantaneous synapses, the firing rates can be expressed as

$$\begin{pmatrix} r_e \\ r_i \end{pmatrix} = \begin{pmatrix} r_{e0} \\ r_{i0} \end{pmatrix} + \begin{pmatrix} a \\ \sqrt{ab} \end{pmatrix} X(T) + \begin{pmatrix} \sqrt{a/b} \\ -1 \end{pmatrix} Y(T), \quad (16)$$

where r_{e0} and r_{i0} are the steady state values of the firing rates right at the bifurcation, $a = \phi'_e J_{ei}/\tau_e$, $b = \phi'_i J_{ie}/\tau_i$, and the slowly evolving variables X and Y evolve on a slow time scale T according to

$$\partial_T X = Y, \quad \partial_T Y = \mu_1 \Delta I_e + \mu_2 \Delta \tau_i Y + cX^2 + dXY, \quad (17)$$

where

$$\mu_1 = \sqrt{\frac{b}{a}} \frac{\phi'_e}{\tau_e}, \quad \mu_2 = \sqrt{ab} \frac{1}{\tau_i},$$

$$c = \phi''_e \sqrt{\frac{b}{a}} \frac{J_{ei}^2}{2\tau_e^3}, \quad d = \phi''_e \frac{J_{ei}}{2\tau_e^2} \left(J_{ee} + J_{ei}\sqrt{\frac{b}{a}} + \frac{J_{ei}}{a\tau_e} \right). \quad (18)$$

See the Appendix for details. Importantly, here the dynamics depend on the two parameters ΔI_e and $\Delta \tau_i$, which are the deviation of the external input to the excitatory neurons and the deviation of the inhibitory time constant from their values right at the TB bifurcation, respectively. The form of the amplitude equations [Eqs. (17)] shows explicitly how the TB bifurcation is intimately related to a SN bifurcation. Fixed points are given by $(X_0, Y_0) = (\pm\sqrt{\mu_1 \Delta I_e/c}, 0)$ and hence there is a SN bifurcation in X for $\Delta I_e = 0$. The two fixed-point solutions near the SN are therefore given by

$$\begin{pmatrix} r_e \\ r_i \end{pmatrix} = \begin{pmatrix} r_{e0} \\ r_{i0} \end{pmatrix} \pm \begin{pmatrix} a \\ \sqrt{ab} \end{pmatrix} \sqrt{\mu_1 \Delta I_e/c}. \quad (19)$$

The stability of these two fixed-point solutions depends on the influence of Y as well. Of the two, one will be stable to steady instabilities, but will destabilize to a Hopf bifurcation (HB) when the inhibitory time constant is sufficiently large. In the case of the SN bifurcation which occurs at high rates, the
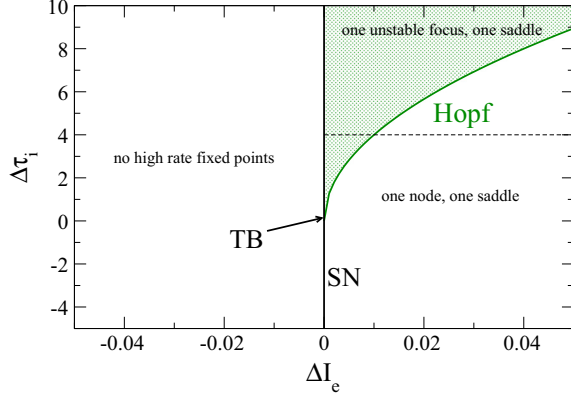
FIG. 6. The phase diagram of fixed-point solutions in the vicinity of the TB bifurcation for the high firing-rate branches in the firing-rate equations [Eqs. (1)] with instantaneous synapses. Parameter values are $J_{ee} = 2$, $J_{ei} = J_{ie} = 1$, $J_{ii} = 0$, $\tau_e = \tau_i = 20$, and $I_i = 1$.

condition can be written as

$$\Delta \tau_i > \frac{d}{\mu_2} X_0, \quad = \frac{d}{\mu_2} \sqrt{\sqrt{\frac{b}{a}} \frac{\phi'_e}{c \tau_e}} \Delta I_e^{1/2}. \tag{20}$$

Again, for the derivation please see the Appendix.

Figure 6 summarizes the types of fixed-point solutions seen in the vicinity of the TB in an E-I network. When we are slightly above the TB bifurcation, for values of $\Delta \tau_i > 0$ there ceases to exist a stable fixed point near the SN; see, e.g., the horizontal, black dashed line in Fig. 6 at $\Delta \tau_i = 4$. Rather, there is an unstable focus. As explained in [24], there are two possibilities in the vicinity of this focus: (1) a stable limit cycle or (2) an unstable limit cycle. Which scenario occurs depends on the sign of the product of the nonlinear coefficients in Eq. (20) c and d. In the Appendix we show that the limit cycle is always *unstable* in Eqs. (17). The solution to the unstable limit cycle near the Hopf Bifurcation can be written $(X, Y) = (1, i\omega)Ae^{i\omega T} + \text{c.c.}$, where A is the amplitude of the unstable limit cycle, the dynamics of which are given by a reduced equation in the vicinity of the Hopf bifurcation (see the Appendix for details), and $\omega = \sqrt{2c X_0}$. Hence, the firing rate of the neurons in the vicinity of the Hopf bifurcation arising from the TB is given by

$$\begin{pmatrix} r_e \\ r_i \end{pmatrix} = \begin{pmatrix} r_{e0} \\ r_{i0} \end{pmatrix} + 2 \begin{pmatrix} \frac{a}{\sqrt{ab}} \end{pmatrix} A \cos \omega T - 2\omega \begin{pmatrix} \sqrt{a/b} \\ -1 \end{pmatrix} A \sin \omega T. \tag{21}$$

Furthermore, this unstable limit cycle disappears via a homoclinic bifurcation [24], and there is therefore no stable large-amplitude limit cycle. The upshot is that near the SN there will be no stable fixed points and no stable limit cycle. Hence, the system will be ejected locally through growing oscillatory fluctuations. For large values of the input, the unstable focus stabilizes and an unstable limit cycle arises.

Figure 7 illustrates how the reduced equations capture the bifurcation structure of the full firing rate equations in the vicinity of the TB. The parameter values are the same as in Fig. 6, with $\Delta \tau_i = 4$; see the dashed, horizontal line in that figure. The two fixed-point branches near the SN, given by
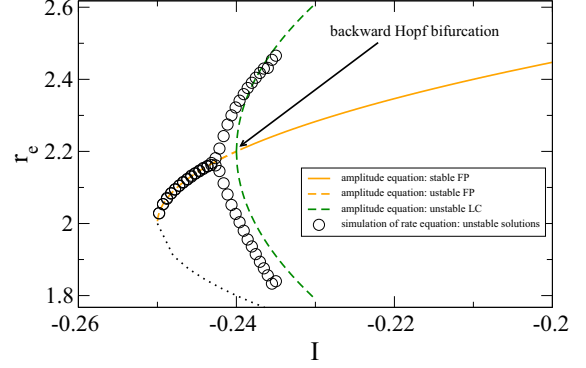

FIG. 7. A bifurcation diagram in the vicinity of the Takens-Bogdanov bifurcation, showing a comparison of the amplitude equation with simulation from the rate model. Parameters are the same as in Fig. 6. The orange and black lines are from Eq. (19) and the dashed green lines are from Eq. (21).

Eq. (19), are shown in orange and black. The orange fixed point is unstable (dashed) until a critical value of the external input is reached, given by condition Eq. (20). The amplitude of the unstable limit cycle is shown by plotting the maximum and minimum of r_e from Eq. (21); see the dashed green lines. Finally, the unstable solutions from simulation of the firing-rate equations Eqs. (1) are shown as open circles.

Finally, let us reiterate that in Fig. 2, as we increase J we are moving ever closer to this double-zero bifurcation point (in the vicinity of the saddle-node lines). Therefore, once we arrive at panel (e), we can be confident that no further changes in the bifurcation diagram will occur.

E. The rate equation with delays and synaptic dynamics

We now consider the rate equations with synapses that exhibit delays and finite rise and decay times, i.e., Eqs. (1)–(3). The fixed points are not altered by the presence of additional time constants or delays. The linear stability of these fixed points, on the other hand, is now given by the full eigenvalue equation, Eq. (5).

The low-frequency limit

In the model without delays, the frequency of the oscillatory instability goes to zero precisely at the saddle-node line. Once delays and synaptic time constants are introduced, they will alter these lines. We can study this by taking the limit of $\lambda = i\omega \to 0$ in Eq. (5). When we do this, we arrive once again at the equations for the Hopf bifurcation, Eqs. (12) to leading order. The only change is the form of the parameter τ, which is now

$$\tau = \frac{(\tau_e + \tau_{d,e} + \tau_{r,e} + D_e)}{(\tau_i + \tau_{d,i} + \tau_{r,i} + D_i)}(1 + J_{ii}). \tag{22}$$

This means that when we include synaptic time constants and delays, the Hopf bifurcation arising from the Takens-Bogdanov point in the vicinity of the saddle-node persists. The only difference is that the effective time constant of excitation and inhibition are now approximately just the linear sum of all of the time constants of each type.
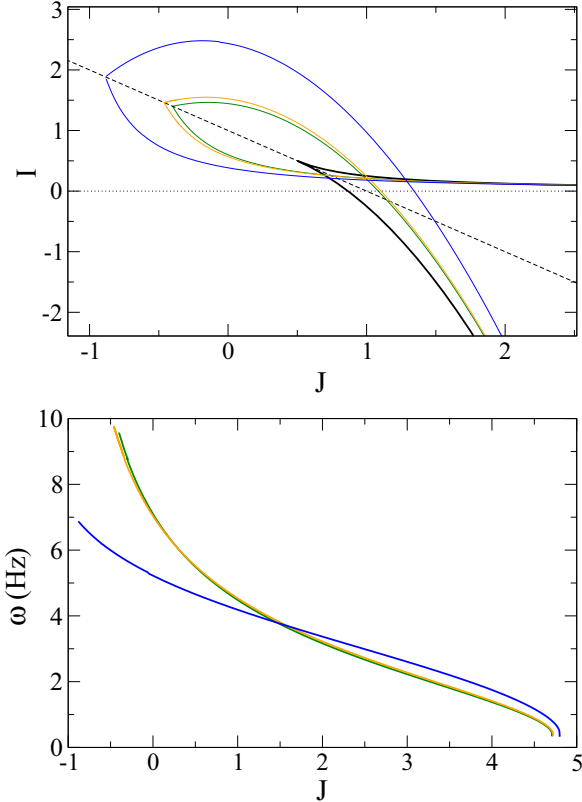
FIG. 8. (Top) The phase diagram with both synaptic delays and synaptic time constants. Here the parameter values are $\beta = 1$, $\tau = 0.2$. The excitatory and inhibitory synaptic time constants and delays are chosen so that the ratio, given by Eq. (22), remains fixed. The green curve is for the case where all synaptic time constants and delays are zero. The orange curve is for $D_e = \tau_{r,e} = \tau_{d,e} = 0.1$, $D_i = \tau_{r,i} = \tau_{d,i} = 1$ and the blue curve is for $D_e = \tau_{r,e} = \tau_{d,e} = 1$, $D_i = \tau_{r,i} = \tau_{d,i} = 10$. (Bottom) The critical frequency along the Hopf-bifurcation line for the different cases.

We can examine the robustness of this asymptotic result numerically by simulating Eqs. (1)–(3). Specifically, if we vary the synaptic time constants but keep the combination τ fixed, we expect that the Hopf line will asymptote to the case without synaptic time constants as the frequency decreases (which means for increasing J). This is shown in the phase diagram Fig. 8, where we have fixed the value $\tau = 0.2$ and also $\beta = 1$ as in Fig. 2. The green curve indicates the Hopf bifurcation lines when there are no synaptic dynamics, and it is therefore identical to the curve in Fig. 2. The orange curve is for $D_e = \tau_{r,e} = \tau_{d,e} = 0.1$, $D_i = \tau_{r,i} = \tau_{d,i} = 1$, and therefore $\tau = 0.2$ and so remains unchanged. The frequency of oscillation along this curve is shown in the bottom panel. If we increase all of the synaptic time constants tenfold, i.e., $D_e = \tau_{r,e} = \tau_{d,e} = 1$, $D_i = \tau_{r,i} = \tau_{d,i} = 10$, the blue curve is found.

III. AN E-I NETWORK OF LEAKY INTEGRATE-AND-FIRE NEURONS

Here we test the robustness of the results in the preceding section, which were derived from a set of firing-rate equations, through analysis and numerical simulation of a network of spiking neurons. We consider an all-to-all connected network of N_E and N_I excitatory and inhibitory leaky integrate-and-fire (LIF) neurons. The membrane potential of a neuron i from population $A \in \{E, I\}$ obeys the following equation:

$$\tau_A \frac{dV_i^A}{dt} = -V_i^A + I_{rec}^A(t) + I_{ext,i}^A(t). \tag{23}$$

Whenever the membrane voltage exceeds a threshold, a spike is emitted and the membrane voltage is reset; i.e., whenever $V_i^A(t^-) = V_t$, then $V_i^A(t^+) = V_r$. The external input current is modeled as $I_{ext,i}^A(t) = \mu_{ext}^A + \sigma_A \sqrt{\tau_A} \eta_i(t)$. That is, there is a constant component plus Gaussian white noise, which is independent from neuron to neuron, i.e., $\langle \eta_i(t)\eta_j(t - t') \rangle = \delta_{ij}\delta(t - t')$. The recurrent input current consists of inhibitory and excitatory synaptic activation, i.e., $I_{rec}^A(t) = I_{syn}^{AE}(t) + I_{syn}^{AI}(t)$, where $I_{syn}^{AB} = \tau_A \frac{J_{AB}}{N_B} s_B(t)$ and the strength of a recurrent synapse from a neuron in population B to a neuron in population A is therefore given by $\frac{J_{AB}}{N_B}$. The synaptic variable s_A obeys the differential equations

$$\tau_A^d \frac{ds_A}{dt} = -s_A + x_A,$$

$$\tau_A^r \frac{dx_A}{dt} = -x_A + \sum_k \sum_{j=1}^{N_A} \delta\left(t - t_j^k - \tau_l^A\right), \tag{24}$$

where the summation is over all spikes emitted by all neurons in population A (all-to-all connected).

This model network can be studied analytically by considering a kinetic formulation of the dynamics [3]. Specifically, all neurons in population A are identical and receive identical inputs except for uncorrelated and independent Gaussian current injection. This allows us to write an evolution equation for the probability distribution of the membrane potential of neurons in a population A with appropriate boundary conditions; see the Appendix for details. From this analysis we can calculate the linear stability of stationary network states, which leads again to Eq. (5). The lone difference with the firing-rate equations is the form of the neural response function, which takes the form of confluent hypergeometric functions [3,25].

Figure 9 shows a phase diagram obtained by solving Eq. (5) numerically for the E-I network of LIF neurons. The bold black curve is the line of SN bifurcations, ending in a cusp near $(\mu_{ext}, J_{ee}) = (-57 \text{ mV}, 38 \text{ mV/ms})$. The thin lines are lines of Hopf bifurcations, for increasing slow inhibitory synaptic kinetics (black, $\tau_i^r = 2$ ms; green, $\tau_i^r = 3$ ms; orange, $\tau_i^r = 4$ ms). When the synaptic inhibition is sufficiently fast, $\tau_i^r = 1$ ms, there is no Hopf bifurcation. The bottom panel shows the frequency of oscillation of the instability along the H curve. Note that the frequency goes to zero for increasing J_{ee} as the H curve approaches the SN line (see the caption for parameter values).

The phase diagram for the network of LIF neurons shown in Fig. 9 is qualitatively similar to the one for the system of firing-rate equations shown in Fig. 2. This suggests that the oscillatory dynamics may also obey the same phenomenology. This is illustrated in Fig. 10. Note the large amplitude oscillations in panels (b) and (c), consistent with a large amplitude limit cycle arising via a subcritical Hopf bifurcation, as in Figs. 2(b)–2(d), while the oscillations in panel (d)
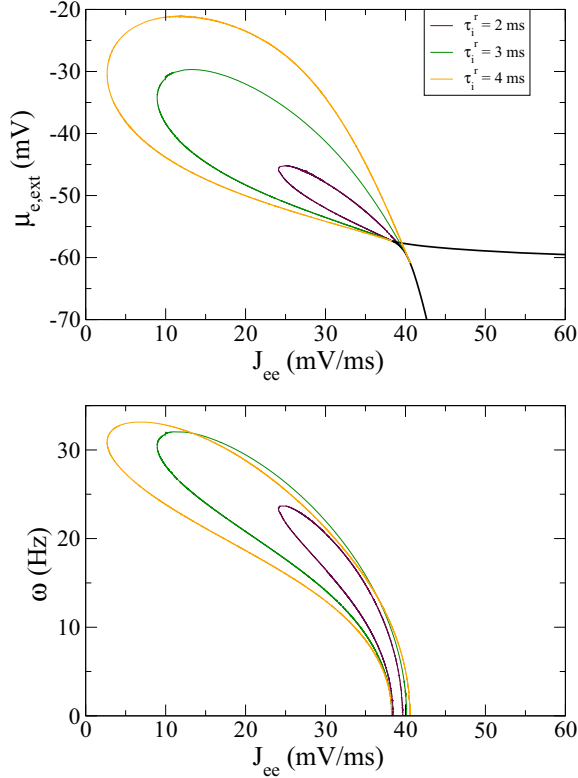
FIG. 9. (Top) The phase diagram for the network of all-to-all connected LIF neurons. Saddle-node (SN) bifurcations occur along the black curve, whereas the colored curves are Hopf bifurcation lines. The maroon, green, and orange curves are for $\tau_i^r = 2$, 3 and 4 ms, respectively. There is no Hopf bifurcation for $\tau_i^r = 1$ ms. (Bottom) The frequency of oscillation of the instability on the Hopf curves. Note how the frequency of oscillation goes to zero as the curves approach the SN, indicating the vicinity of a Takens-Bogdanov bifurcation. Other parameters are $\tau_e^r = 1$ ms, $\tau_e^d = \tau_e^d = 10$ ms, $\tau_e = 20$ ms, $\tau_i = 10$ ms, $\tau_r = 1$ ms, $J_{ei} = J_{ie} = 30$ mV/ms, $J_{ii} = 20$ mV/ms, $I_{ext}^I = -60$ mV/ms, $\sigma_e = \sigma_i = 5$ mV, $V_t = -55$ mV, and $V_r = -65$ mV.

are much more irregular, consistent with damped noise-driven oscillations [and with Fig. 2(e)] and hence with the phenomenology of the Takens-Bogdanov bifurcation.

The noise-driven damped oscillations due to the proximity of the TB bifurcation can lead to a broad increase in power at low frequencies in the power spectrum of the spiking activity. This is illustrated in Fig. 11. Figure 11(a) shows a bifurcation diagram of the firing rate of E neurons in the bistable regime in the network of LIF neurons. Figure 11(b) shows sample traces of sustained, working-memory-like behavior for two sets of parameter values, and the power spectra of this activity is shown in Fig. 11(c). Note that the spectrum of the orange trace, for which there is no instability, nonetheless shows a large increase in power in the 1–10-Hz range (δ to θ) [26]. Damped oscillations at higher frequencies can also be obtained near the TB bifurcation; see Fig. 12 for an example of low-β oscillations.

Once a Hopf bifurcation occurs in the vicinity of the SN bifurcation, the effective range of inputs for which there is bistability is reduced. Therefore, when the network activity is in the low-activity state in the bistable regime, a transient

input will not necessarily lead to sustained activity. In the firing-rate equation, transient inputs in this regime lead to an all-or-none response of the network to population bursts; see Fig. 4. In the network of LIF neurons, similar dynamics are seen, although the response is more heterogeneous depending on the strength of the input. This is illustrated in Fig. 13, where sufficiently strong inputs lead to all-or-none population bursts [green and black dashed lines in Fig. 13(b)], whereas more moderate inputs can lead to more complex responses [violet and orange in Fig. 13(b)].

IV. DISCUSSION

In this paper we have studied the phenomenology of oscillations in the bistable regime of E-I networks. Oscillations emerge generically in E-I networks via an oscillatory (Hopf) instability and have been studied extensively both numerically and analytically [3,5,27,28]. These studies, as well as related work on the response of spiking networks to weak external stimuli, e.g., [25], make the implicit assumption that the network is far from a "working memory" regime in which several stable stationary states coexist. When this is no longer the case, the Hopf instability leading to oscillations and the steady instability leading to bistability of fixed points must be considered together. The dynamics which result from the interaction of these two types of instabilities can be understood by considering a reduced description of the system in which they co-occur, known as a TB bifurcation [24]. This description predicts that when the firing rate first becomes unstable to oscillations, there is, in fact, no stable limit cycle solution. This has two main consequences for neuronal activity: (1) population bursts robustly occur (see Figs. 4, 5, and 13) and (2) oscillations during working memory states are noise driven (not limit cycles) and hence broadband. Oscillations emerging from the TB bifurcation can, in principle, exhibit arbitrarily low frequencies, although in network simulations they robustly occur in the δ to γ range; see Figs. 11 and 12 for examples of δ and θ and β.

Interestingly, the dynamical regime of neuronal networks near the TB point is related to the so-called inhibition stabilized network regime (ISN) discussed in [29]. In that work, it was noted that eigenvalues of the linearization of a network of excitatory and inhibitory neurons about a fixed point are not orthogonal. The consequence of this is that certain perturbations can lead to transient amplification of the activity, even though the fixed point is linearly stable. The authors showed that the linearized system could be rewritten in terms of a difference and a summation mode, revealing a hidden feedforward structure: Perturbations of the difference mode caused transient amplification of the summation mode. An analogous feedforward structure is clearly visible in the normal form for the TB [Eqs. (17)]. In particular, the variable Y, which represents the amplitude of perturbations of the scaled difference between the excitatory and inhibitory populations, drives X, a summation mode; see Eq. (16). In contrast with the ISN, networks at the TB point are not linearly stable and hence nonlinear effects must be considered, i.e., the quadratic terms in Eq. (13). Therefore, the TB represents the dynamics of an ISN in the limit in which the recurrent excitation is strong enough to overcome the stabilizing effects of the
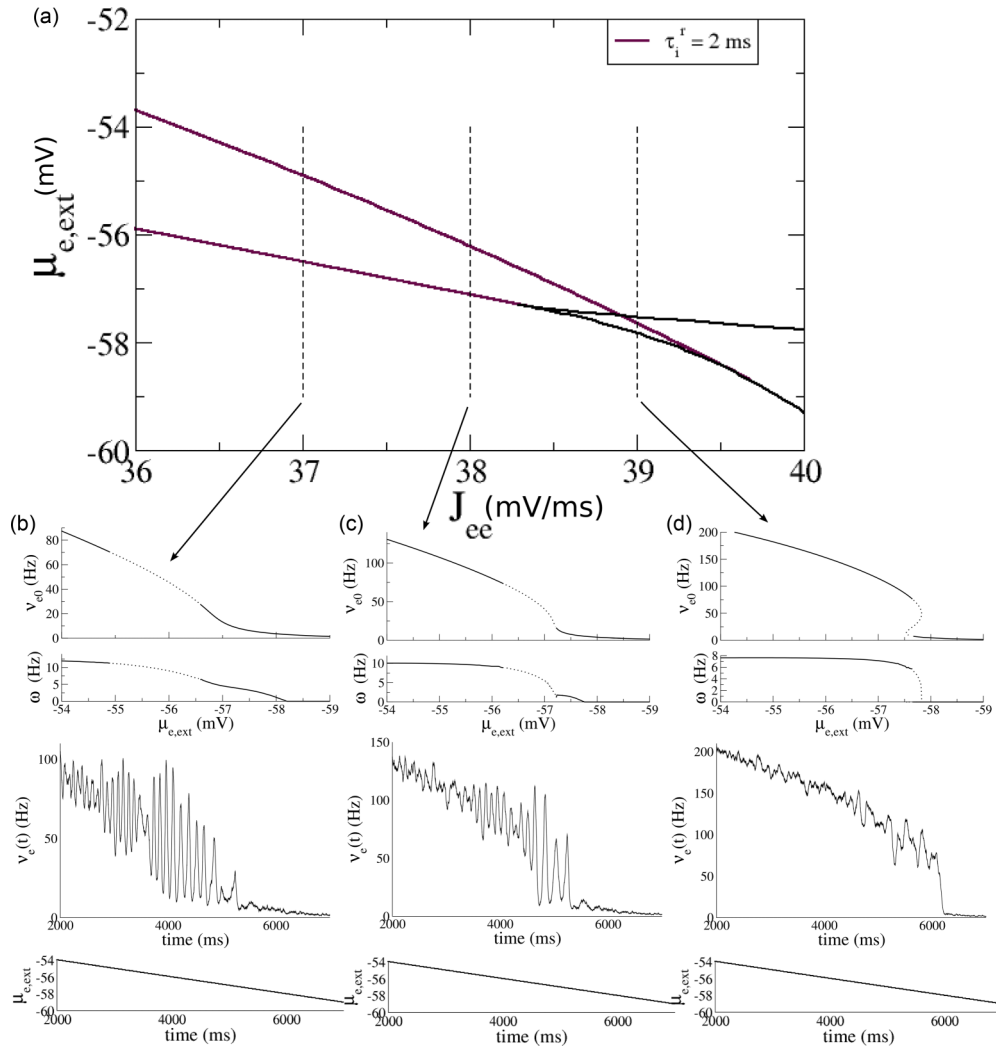
FIG. 10. A magnification of the phase diagram from Fig. 9(a) and illustrative bifurcation diagrams and corresponding dynamics from numerical simulations (b)–(d). The phase diagram shows the line of SN bifurcations (black) and a line of H bifurcations for $\tau_i^r = 2$ ms (maroon). The vertical dashed lines indicate the values of the recurrent excitatory synaptic weights $J_{ee} = 37$, 38, and 39 mV/ms and the ranges of external input $\mu_{e,ext} \in [-54, -59]$ mV used for the bifurcation diagrams and numerical simulations shown in (b)–(d). (b) (Top) The bifurcation diagram for $J_{ee} = 37$ mV/ms showing the stationary firing rate ν_{e0} of the excitatory population and the frequency ω of the most unstable eigenvalue, both calculated from the dispersion equation for the network of LIF neurons. Below this diagram is the firing rate of the E neurons from a numerical simulation in which the external input is ramped down across the range of values from the bifurcation diagram. (c) and (d) Same as (b), but for $J_{ee} = 38$ and 39 mV/ms. All parameter values are the same as in Fig. 9.

inhibition. There is growing evidence that neuronal circuits in the visual cortex operate as an ISN [29,30]. Our results suggest that ISN dynamics may also be associated with saddle-node bifurcations typically linked to association cortex functions, e.g., working memory and decision making, when recurrent excitation is strong enough and the circuit operates near a TB point.

Our approach in this paper has been to analyze the dynamics near a TB point in a simplified firing-rate model and then confirm this analysis in networks of spiking neurons. The phase diagrams delineating different dynamical regimes are qualitatively similar in the two models; compare, for example, the phase diagrams in Figs. 2 and 9. Indeed, heuristic firing-rate equations provide a good qualitative description of emergent dynamical states in spiking networks even when there is significant quenched variability and even for complex

spatiotemporal patterns, e.g., [23,31,32], although they fail to describe the response of the network to external drive when spike synchrony is important [20,33]. In general, important differences in the dynamics between rate equations and spiking networks can arise when the dynamics is nonstationary. An example of this can be seen in the complex transient response to pulses in the network shown in Fig. 13, compared to the simple all-or-none response in the rate equation shown in Fig. 4. Therefore, although both models exhibit large-amplitude excursions in the firing rate in the vicinity of the TB in response to transient inputs, a qualitative validation of the analysis from the simplified model, the spiking network shows more complexity in response duration. We have not studied these differences in any detail here.

The existence of a TB bifurcation in the Wilson-Cowan equations was first mentioned by Borisyuk and Kirrilov [34].
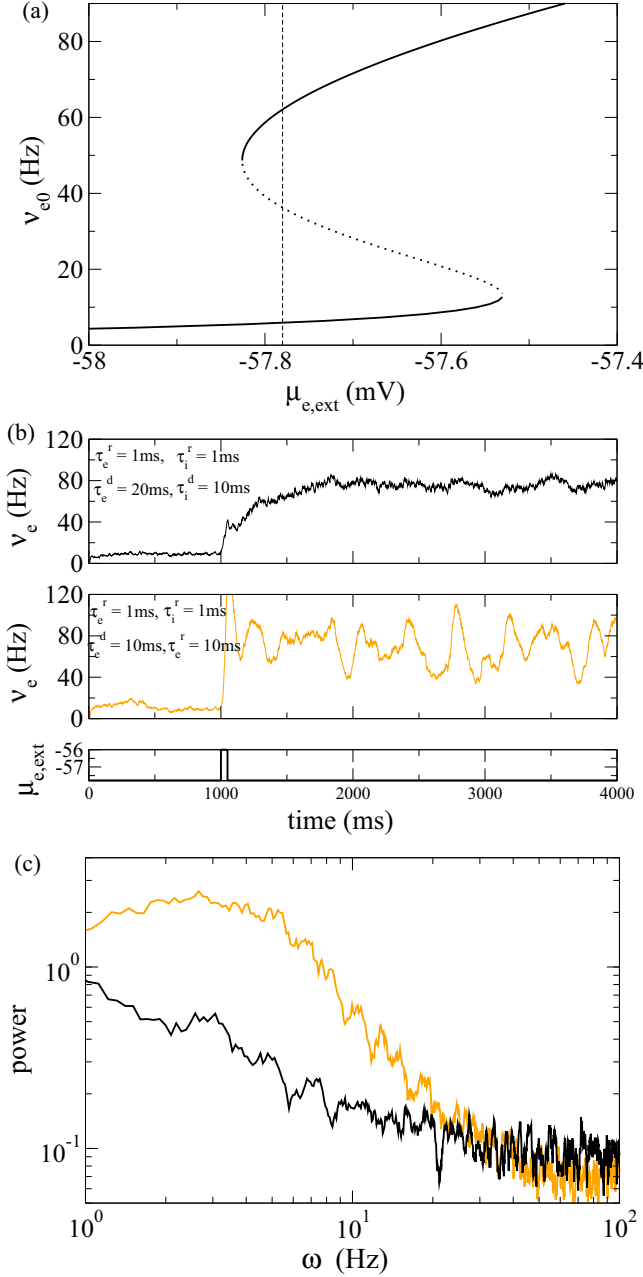
FIG. 11. Oscillatory fluctuations in the bistable regime in the δ and θ ranges. (a) A bifurcation diagram given the same parameters as in Fig. 9 and with $J_{ee} = 39$ mV/ms for the case when there is no Hopf bifurcation, i.e., oscillatory modes are damped. (b) Examples of sustained activity in the bistable regime for $\mu_{e,ext} = -57.78$ mV [see vertical dotted line in panel (a)]. The black trace is for slow excitation: $\tau_e^r = \tau_i^r = 1$ ms, $\tau_e^d = 20$ ms, $\tau_i^d = 10$ ms. In this case oscillations are very strongly damped. The orange trace is for the same parameters except $\tau_e^d = 10$ ms. (c) The power spectra for 10-s traces of sustained activity for the traces shown above.

Despite this, the significance of the TB for neuronal dynamics has not been discussed or analyzed in detail elsewhere. Here we explicitly derived the normal form equation for the TB from the firing-rate equations [Eqs. (1)]. From the normal form we showed that the Hopf bifurcation leads to an unstable, small-amplitude limit cycle. This unstable limit cycle, in turn,
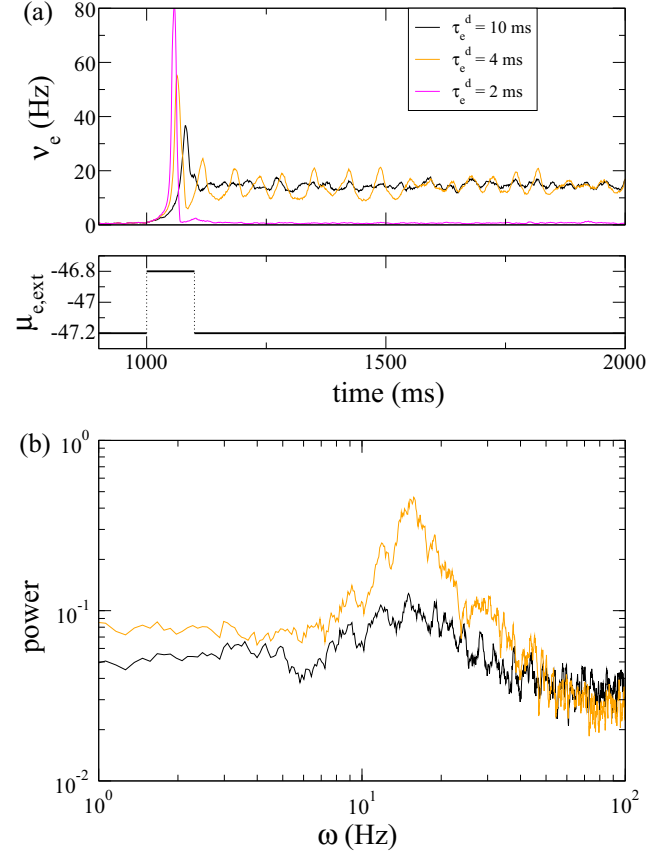

FIG. 12. Oscillatory fluctuations in the bistable regime in the low-β range. (a) The firing rate of the excitatory population in response to a transient input at $t = 1000$ ms and for three values of τ_e^d: 10 ms (black), 4 ms (orange), and 2 ms (violet). Note that when $\tau_e^d = 2$ ms the upper branch is unstable and the response is a population burst. Parameters: $I_{i,ext} = -48.3$ mV, $J_{ee} = 10$ mV/ms, $J_{ie} = 20$ mV/ms, $J_{ei} = J_{ii} = 3$ mV, $\tau_e^r = \tau_i^r = \tau_i^d = 1$ ms, $\tau_e = 20$ ms, $\tau_i = 10$ ms, $\tau_r = 1$ ms, $V_t = -55$ mV, $V_r = -59$ mV.

vanishes in a homoclinic bifurcation of the saddle point [see Figs. 2(e) and 7] with the consequence that over a range of external input values there is no stable attractor, oscillatory or otherwise, at "high" rates; the activity drops to the stable lower branch in this range. This suggests that physiological effects or external manipulations which promote oscillations in the E-I loop may disrupt working-memory states; e.g., see [35]. More generally, slow oscillations due to the E-I loop can serve as electrophysiological biomarkers of networks operating in the bistable regime: Hyperactivity in such networks (leaving the bistable regime through excess excitation) is accompanied by a decrease in oscillation amplitude and an increase in oscillation frequency, while hypoactivity with an increase in oscillation amplitude and a decrease in frequency [36]. We have recently suggested that this mechanism may account for the θ-band EEG being a biomarker of treatment outcome in patients suffering major depression [36].
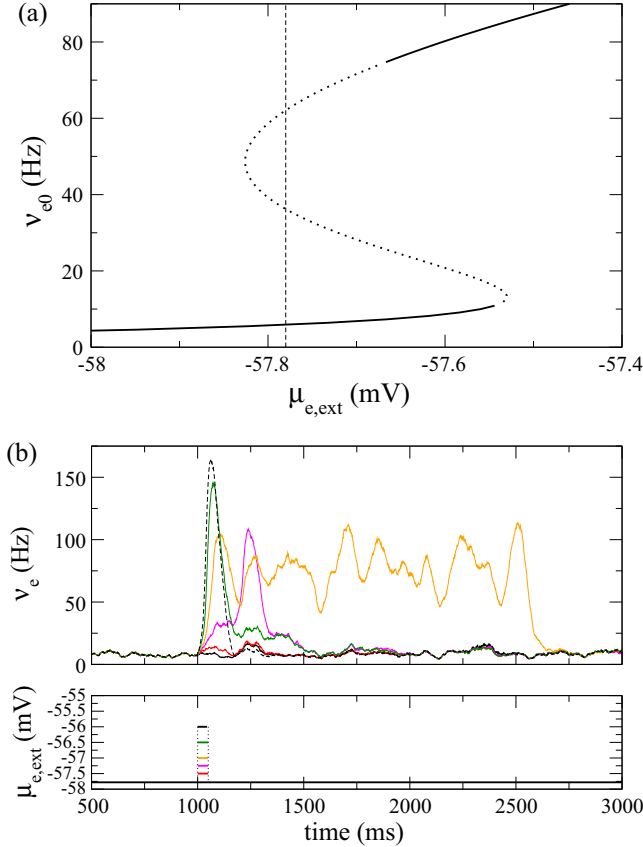
FIG. 13. The response of the network of LIF neurons to transient inputs in the bistable regime with unstable oscillations. (a) The bifurcation diagram for $\tau_e^r = 1$ ms, $\tau_i^r = 2$ ms, $\tau_e^d = \tau_i^d = 10$ ms. All other parameters are the same as in Fig. 9. The vertical dashed line shows the value of the input used for the simulations in (b). (b) Sample traces of the excitatory firing rate for different amplitudes of a transient input given from 1000 to 1050 ms. The color code from smallest to largest amplitude: black, red, violet, orange, green, black (dashed).

APPENDIX

1. Amplitude equation for oscillations in the E-I rate equations without synaptic dynamics

In this section we calculate an equation for the amplitude of oscillations arising from a Hopf instability a system of firing rate equations for an E-I network. The equations are

$$\tau_e \dot{r}_e = -r_e + \phi(J_{ee}r_e - J_{ei}r_i + I_e),$$
$$\tau_i \dot{r}_i = -r_i + [J_{ie}r_e - J_{ii}r_i + I_i]_+,$$
(A1)

where $[x]_+ = x$ if $x > 0$ and is zero otherwise. The fixed-point solution of this system of equations can be written $\mathbf{r}_0 = (r_{e0}, r_{i0})$.

To determine the dynamics of the amplitude of the oscillations, we expand the rates as $\mathbf{r} = \mathbf{r}_0 + \epsilon \mathbf{r}_1 + \epsilon^2 \mathbf{r}_2 + \cdots$,

where $\epsilon \ll 1$ is a small parameter defined by the distance from the value of the external input to E neurons at the bifurcation, i.e., $I_e = I_{e0} + \epsilon^2 \Delta I_e$. We also define a slow time $T = \epsilon^2 t$ and so $\partial_t \to \partial_t + \epsilon \partial_T$. Expanding in orders of ϵ we find

$$(\mathcal{L} + \epsilon^2 \mathcal{L}_2)(\epsilon \mathbf{r}_1 + \epsilon^2 \mathbf{r}_2 + \cdots) = \epsilon^2 N_2 + \epsilon^3 N_3 + \cdots,$$
(A2)

where

$$\mathcal{L} = \begin{pmatrix} \tau_e \partial_t + 1 - J_{ee}\phi' & J_{ei}\phi' \\ -J_{ie} & \tau_i \partial_t + 1 + J_{ii} \end{pmatrix},$$

$$\mathcal{L}_2 = \begin{pmatrix} \tau_e \partial_T & 0 \\ 0 & \tau_i \partial_T \end{pmatrix},$$

$$N_2 = \begin{pmatrix} \frac{\phi''}{2}(J_{ee}r_{e1} - J_{ei}r_{i1})^2 + \phi' \Delta I_e \\ 0 \end{pmatrix},$$
(A3)

$$N_3 = \begin{pmatrix} \phi''(J_{ee}r_{e1} - J_{ei}r_{i1})(J_{ee}r_{e2} - J_{ei}r_{i2} + \Delta I_e) \\ 0 \end{pmatrix}$$
$$+ \begin{pmatrix} \frac{\phi'''}{6}(J_{ee}r_{e1} - J_{ei}r_{i1})^3 \\ 0 \end{pmatrix}.$$

$O(\epsilon)$:
At this order we have the linear stability condition

$$\mathcal{L}\mathbf{r}_1 = 0.$$
(A4)

The solution to these equations at an oscillatory instability is $\mathbf{r}_1 = (r_{e1}, r_{i1}) = (\tilde{r}_{e1}, \tilde{r}_{i1})A(T)e^{i\omega t} + $ c.c., where ω is given by Eq. (13), $(\tilde{r}_{e1}, \tilde{r}_{i1}) = (-J_{ei}\phi', i\tau_e\omega + 1 - J_{ee}\phi')$, and $A(T)$ is a slowly varying amplitude. We also need the left-null eigenvector $\mathbf{r}^\dagger$, where $\mathbf{r}\mathcal{L} = 0$. It is $\mathbf{r}^\dagger = (J_{ie}, -i\tau_e\omega + 1 - J_{ee}\phi')e^{i\omega t}$.

$O(\epsilon^2)$:

$$\mathcal{L}\mathbf{r}_2 = N_2.$$
(A5)

Making use of the solution $\mathbf{r}_1$ from the previous order, we can write

$$N_2 = \begin{pmatrix} J_{ei}^2 \phi''(1 + \tau_e^2 \omega^2)|A|^2 + \phi' \Delta I_e \\ 0 \end{pmatrix}$$
$$+ \begin{pmatrix} J_{ei}^2 \frac{\phi''}{2}(1 + i\tau_e\omega)^2 A^2 \\ 0 \end{pmatrix} e^{2i\omega t} + \text{c.c.}$$
(A6)

The solution of Eqs. (A5) is $\mathbf{r}_2 = \mathbf{r}_{20} + (\mathbf{r}_{22}e^{2i\omega t} + \text{c.c.})$, where

$$\mathbf{r}_{20} = (1 + J_{ii}, J_{ie})^T \cdot \frac{\phi'' J_{ei}^2(1 + \tau_e^2 \omega^2)|A|^2 + \phi' \Delta I_e}{\tau_e \tau_i \omega^2},$$

$$\mathbf{r}_{22} = -(2i\tau_i\omega + 1 + J_{ii}, J_{ie})^T \cdot \frac{\phi'' J_{ei}^2(1 + i\tau_e\omega)^2 A^2}{6\tau_e \tau_i \omega^2}.$$ (A7)

$O(\epsilon^3)$:

$$\mathcal{L}\mathbf{r}_3 + \mathcal{L}_2\mathbf{r}_1 = N_3.$$
(A8)

At this order we note that the nonlinear term N_3 generates terms proportional to $\mathbf{r}_1$. These secular terms must be eliminated in order to solve for $\mathbf{r}_3$. This is done by applying the solvability condition

$$\langle \mathbf{r}^\dagger, \mathcal{L}_2\mathbf{r}_1 \rangle = \langle \mathbf{r}^\dagger, N_3 \rangle,$$
(A9)

where $\langle x, y \rangle = \int dt(x^* \cdot y)$, and we have used $\langle \mathbf{r}^\dagger, \mathcal{L}r \rangle = 0$, for any r.

Using the results from the last two orders we find

$$N_3 = \begin{pmatrix} -1 \\ 0 \end{pmatrix} \bigg[\phi'' J_{ei}(1 + i\tau_e\omega)A(J_{ee}r_{e20} - J_{ei}r_{e20} + \Delta I_e)$$

$$+ \phi'' J_{ei}(1 - i\tau_e\omega)A^*(J_{ee}r_{e22} - J_{ei}r_{i22})$$

$$+ \frac{\phi'''}{2} J_{ei}^3 (1 + \tau_e^2\omega^2)(1 + i\tau_e\omega)|A|^2 A \bigg] e^{i\omega t} + \cdots,$$
$$\tag{A10}$$

and, finally, Eq. (A9) yields the equation

$$\tau_e\partial_T A = \frac{J_{ei}J_{ie}(1 + i\tau_e\omega)}{2\tau_e\omega[\tau_i\omega + i(1 + J_{ii})]}[\mu\Delta I_e A + c|A|^2 A],$$

$$\mu = \phi'' \left[1 + \frac{\phi'(1 + J_{ii})J}{\tau_e\tau_i\omega^2} \right],$$

$$c = J_{ei}^2 (1 + \tau_e^2\omega^2) \left[\frac{5}{6} \frac{(\phi'')^2(1 + J_{ii})}{\tau_e\tau_i\omega^2} J + \frac{\phi'''}{2} \right.$$

$$\left. - \frac{i}{3\omega}(\phi'')^2 J_{ee} \right].$$
$$\tag{A11}$$

Whether the oscillations are subcritical or supercritical depends on the sign of the real part of the cubic term c. They are subcritical when the inequality Eq. (15) is satisfied. Note also that the dynamics blows up in the limit $\omega \to 0$, i.e., in the vicinity of the SN bifurcation. In this limit one must rescale the firing rates and take into account the fact that there are two near-zero eigenvalues to obtain the correct equations. We do this in the next section.

2. Amplitude equation for the Takens-Bogdanov bifurcation

Again we consider the firing-rate equations Eqs. (A1), although we rewrite them slightly to obtain

$$\dot{r}_e = -\frac{r_e}{\tau_e} + \frac{1}{\tau_e}\phi(J_{ee}r_e - J_{ei}r_i + I_e),$$

$$\dot{r}_i = -\frac{r_i}{\tau_i} + \frac{1}{\tau_i}[J_{ie}r_e - J_{ii}r_i + I_i]_+.$$
$$\tag{A12}$$

At the TB bifurcation point, there are two zero eigenvalues of the linearized system; i.e., both conditions Eqs. (7) and (8) hold. These conditions greatly simplify the form of the linearized system.

Once again we expand the firing rates in a small parameter ϵ, which measures the distance from the TB bifurcation. The expansion is $\mathbf{r} = \mathbf{r}_0 + \epsilon\mathbf{r}_1 + \epsilon^{3/2}\mathbf{r}_2 + \epsilon^2\mathbf{r}_3 + \epsilon^{5/2}\mathbf{r}_4 + \cdots$. We take $I_e = I_{e0} + \epsilon^2\Delta I_e$, $\tau_i = \tau_{i0} + \epsilon\Delta\tau_i$ and define the slow time $T = \epsilon^{1/2}t$. Plugging these expansions into Eqs. (A12) and using Eqs. (7)–(8), we can write

$$(\mathcal{L} + \epsilon^{1/2}\mathcal{L}_1 + \epsilon\mathcal{L}_2)(\epsilon\mathbf{r}_1 + \epsilon^{3/2}\mathbf{r}_2 + \cdots)$$
$$= \epsilon^2 N_2 + \epsilon^{5/2} N_3 + \cdots,$$
$$\tag{A13}$$

where

$$\mathcal{L} = \begin{pmatrix} \partial_t - \sqrt{ab} & a \\ -b & \partial_t + \sqrt{ab} \end{pmatrix}, \quad \mathcal{L}_1 = \begin{pmatrix} \partial_T & 0 \\ 0 & \partial_T \end{pmatrix},$$

$$\mathcal{L}_2 = \begin{pmatrix} 0 & 0 \\ b & -\sqrt{ab} \end{pmatrix} \frac{\Delta\tau_i}{\tau_{i0}},$$

$$N_2 = \begin{pmatrix} \frac{\phi''}{2\tau_e}(J_{ee}r_{e1} - J_{ei}r_{i1})^2 + \frac{\phi'}{\tau_e}\Delta I_e \\ 0 \end{pmatrix},$$

$$N_3 = \begin{pmatrix} \frac{\phi''}{\tau_e}(J_{ee}r_{e1} - J_{ei}r_{i1})(J_{ee}r_{e2} - J_{ei}r_{i2}) \\ 0 \end{pmatrix},$$
$$\tag{A14}$$

and where $a = \phi'_e J_{ei}/\tau_e$ and $b = J_{ie}/\tau_{i0}$.

$O(\epsilon)$:

$$\mathcal{L}\mathbf{r}_1 = 0.$$
$$\tag{A15}$$

The solution is $\mathbf{r}_1 = \mathbf{e}_1 X(T)$, where $\mathbf{e}_1 = (a, \sqrt{ab})$ is the right null eigenvector of $\mathcal{L}$ and $X(T)$ is a slowly varying amplitude. The left null eigenvector of the matrix $\mathcal{L}$ satisfies

$$\mathcal{L}^T \mathbf{r}_1^\dagger = 0$$
$$\tag{A16}$$

and can be taken as $\mathbf{r}_1^\dagger = (b, -\sqrt{ab})$.

$O(\epsilon^{3/2})$:

$$\mathcal{L}\mathbf{r}_2 = -\mathcal{L}_1\mathbf{r}_1, \quad = -\mathbf{e}_1\partial_T X,$$
$$\tag{A17}$$

which indicates that the action of the linearized operator on $\mathbf{r}_2$ is to rotate it parallel to the right null eigenvector. This is one way of defining a *generalized* right null eigenvector $\mathbf{e}_2$, for which $\mathcal{L}^2\mathbf{e}_2 = 0$. One choice for this eigenvector is $\mathbf{e}_2 = \frac{1}{2}(\sqrt{a/b}, -1)$. If we choose $\mathbf{r}_2 = \mathbf{e}_2 Y(T)$, where $Y(T)$ is a slowly varying amplitude we find that $\partial_T X = Y$. The generalized left-null eigenvector $\mathbf{e}_2^\dagger$ for which $\mathcal{L}^T\mathbf{e}_2^\dagger = \mathbf{e}_1^\dagger$ can be taken to be $\mathbf{e}_2^\dagger = -\frac{1}{2}(\sqrt{b/a}, 1)$

$O(\epsilon^2)$:

$$\mathcal{L}\mathbf{r}_3 + \mathcal{L}_1\mathbf{r}_2 + \mathcal{L}_2\mathbf{r}_1 = \mathbf{N}_2,$$
$$\tag{A18}$$

where

$$\mathbf{N}_2 = \begin{pmatrix} \frac{\phi''_e J_{ei}^2}{2\tau_e^3} X^2 + \frac{\phi'_e}{\tau_e}\Delta I_e \\ 0 \end{pmatrix}.$$
$$\tag{A19}$$

We project Eq. (A18) onto the left-null eigenspace of $\mathcal{L}$ to eliminate secular terms. That is, we must solve

$$\langle \mathbf{e}_1^\dagger, \mathcal{L}_1\mathbf{r}_2 \rangle = \langle \mathbf{e}_1^\dagger \mathbf{N}_2 \rangle,$$
$$\tag{A20}$$

where the term proportional to $\mathcal{L}$ vanishes by the definition of $\mathbf{e}_1^\dagger$ and the term proportional to $\mathcal{L}_2$ is identically zero. Here $\langle x, y \rangle = x^T \cdot y$ is a dot product. Solving this equation yields

$$\sqrt{ab}\partial_T Y = \frac{b\phi'_e}{\tau_e}\Delta I_e + \frac{b\phi''_e J_{ei}^2}{2\tau_e^3} X^2.$$
$$\tag{A21}$$

In order to solve for $\mathbf{r}_3$, we project onto the generalized left-null eigenspace

$$\langle \mathbf{e}_2^\dagger, \mathcal{L}\mathbf{r}_3 \rangle = \langle \mathbf{e}_2^\dagger, \mathbf{N}_2 \rangle,$$
$$\tag{A22}$$

which yields

$$-br_{e3} + \sqrt{ab}r_{i3} = \frac{1}{2}\sqrt{\frac{b}{a}}\frac{\phi'_e}{\tau_e}\Delta I_e + \frac{1}{2}\sqrt{\frac{b}{a}}\frac{\phi''_e J_{ei}^2}{2\tau_e^3} X^2. \tag{A23}$$

$O(\epsilon^{5/2})$:

$$\mathcal{L}\mathbf{r}_4 + \mathcal{L}_1\mathbf{r}_3 + \mathcal{L}_2\mathbf{r}_2 = \mathbf{N}_3.$$
$$\tag{A24}$$

We project onto the left-null eigenspace to obtain

$$\langle \mathbf{e}_1^\dagger, \mathcal{L}_1\mathbf{r}_3 \rangle + \langle \mathbf{e}_1^\dagger, \mathcal{L}_2\mathbf{r}_2 \rangle = \langle \mathbf{e}_1^\dagger, \mathbf{N}_3 \rangle,$$
$$\tag{A25}$$

where

$$\mathbf{N}_3 = \begin{pmatrix} \frac{\phi_e'' J_{ei}}{2\tau_e^2}(J_{ee}\sqrt{a/b} + J_{ei})XY \\ 0 \end{pmatrix}. \qquad (A26)$$

This yields

$$-\sqrt{\frac{b}{a}}\frac{\phi_e'' J_{ei}^2}{2\tau_e^3}XY - ab\frac{\Delta\tau_i}{\tau_{i0}}Y = \frac{b\phi_e'' J_{ei}}{2\tau_e^2}(J_{ee}\sqrt{a/b} + J_{ei})XY. \qquad (A27)$$

Finally, collecting terms at orders up to $\epsilon^{5/2}$ yields the coupled amplitude equations Eqs. (17).

3. Amplitude equation for the Hopf bifurcation near the Takens-Bogdanov bifurcation

In this section we show that the Hopf bifurcation in the vicinity of the TB is always backward, indicating that the limit cycle which arises is unstable. We first consider the linear stability of fixed-point solutions in Eqs. (17). We note first that the sign of the nonlinear coefficients c and d depends only on the sign of the curvature of the transfer function ϕ_e''. The sign is negative for high rates (when the transfer function is a square root) and positive for low rates (when it is quadratic). Fixed-point solutions are given by $\mathbf{X} = \mathbf{X}_0 = (\pm\sqrt{-\frac{\mu_1\Delta I_e}{c}},0)$, and hence two solutions appear for $\Delta I_e > 0$ when $c < 0$ (high rate) and for $\Delta I_e < 0$ when $c > 0$ (low rate).

The linear stability is found by perturbing about the fixed-point solutions $\mathbf{X} = \mathbf{X}_0 + \delta\mathbf{X}e^{\lambda t}$ and plugging into Eqs. (17), where $\delta\mathbf{X} \ll 1$. This yields the characteristic equation $\lambda^2 + \lambda(-\mu_2\Delta\tau_i - dX_0) - 2cX_0 = 0$. There is an oscillatory instability when $\lambda = i\omega$, which occurs when $\Delta\tau_i = \frac{-dX_0}{\mu_2}$, and $\omega = \sqrt{-2cX_0}$. Note that the combinations $dX_0 > 0$ and $cX_0 > 0$ for the relevant branch (the other is a saddle).

We conduct a weakly nonlinear analysis for this oscillatory instability by expanding the variables $\mathbf{X} = \mathbf{X}_0 + \epsilon\mathbf{X}_1 + \epsilon^2\mathbf{X}_2 + \cdots$, where the small parameter ϵ measures the distance to the bifurcation and is given by $\Delta I_e = \Delta I_{e0} + \epsilon^2\Delta I_{e1}$. We define a slow time $\tau = \epsilon^2 T$. Plugging these expansions into Eqs. (17), we can write

$$(\mathcal{L} + \epsilon^2\mathcal{L}_2)(\epsilon\mathbf{r}_1 + \epsilon^2\mathbf{r}_2 + \cdots) = \epsilon^2\mathbf{N}_2 + \epsilon^3\mathbf{N}_3, \qquad (A28)$$

where

$$\mathcal{L} = \begin{pmatrix} \partial_T & -1 \\ \omega^2 & \partial_T \end{pmatrix}, \quad \mathcal{L}_2 = \begin{pmatrix} \partial_\tau & 0 \\ 0 & \partial_\tau \end{pmatrix},$$

$$\mathbf{N}_2 = \begin{pmatrix} 0 \\ cX_1^2 + dX_1Y_1 \end{pmatrix},$$

$$\mathbf{N}_3 = \begin{pmatrix} 0 \\ 2cX_1X_2 + d(X_1Y_2 + X_2Y_1) \end{pmatrix}. \qquad (A29)$$

$O(\epsilon)$:

$$\mathcal{L}\mathbf{X}_1 = 0. \qquad (A30)$$

The solution for an oscillatory instability is $\mathbf{X}_1 = \mathbf{e}A(\tau)e^{i\omega T} + $ c.c., where the right null eigenvector $\mathbf{e} = (1,i\omega)$ and A is a slowly varying amplitude. The left null eigenvector is $\mathbf{e}^\dagger = (\omega^2,i\omega)e^{i\omega t}$.

$O(\epsilon^2)$:

$$\mathcal{L}\mathbf{X}_2 = \mathbf{N}_2. \qquad (A31)$$

Using the solution $\mathbf{X}_1$ from last order, we can express the nonlinear forcing as

$$\mathbf{N}_2 = \begin{pmatrix} 0 \\ c + id\omega \end{pmatrix}A^2e^{2i\omega t} + \text{c.c.} + \begin{pmatrix} 0 \\ 2c|A|^2 + \Delta I_{e1} \end{pmatrix}. \qquad (A32)$$

From this we find that the solution at this order can be written $\mathbf{X}_2 = \mathbf{X}_{22}A^2e^{2i\omega t} + \text{c.c.} + \mathbf{X}_{20}$, where

$$\mathbf{X}_{22} = -\frac{(c + id\omega)}{3\omega^2}\begin{pmatrix} 1 \\ 2i\omega \end{pmatrix},$$

$$\mathbf{X}_{20} = \frac{1}{\omega^2}\begin{pmatrix} 2c|A|^2 + \Delta I_{e1} \\ 0 \end{pmatrix}. \qquad (A33)$$

$O(\epsilon^3)$:

$$\mathcal{L}\mathbf{X}_3 + \mathcal{L}_2\mathbf{X}_1 = \mathbf{N}_3, \qquad (A34)$$

where

$$\mathbf{N}_3 = \frac{1}{\omega^2}\begin{pmatrix} 0 \\ 2c + id\omega \end{pmatrix}\Delta I_{e1}Ae^{i\omega t}$$
$$+ \frac{1}{\omega^2}\begin{pmatrix} 0 \\ \frac{10}{3}c^2 + \frac{1}{3}d^2\omega^2 + icd\omega \end{pmatrix}$$
$$\times |A|^2Ae^{i\omega t} + \text{c.c.} + \cdots, \qquad (A35)$$

where we have only written the terms proportional to $e^{i\omega t}$. These are secular terms which must be eliminated for a bounded solution to exist at this order. This is done by projecting onto the left null eigenvector of the linearized matrix $\mathcal{L}$, i.e.,

$$\langle \mathbf{X}^\dagger, \mathcal{L}_2\mathbf{X}_1 \rangle = \langle \mathbf{X}^\dagger, \mathbf{N}_3 \rangle, \qquad (A36)$$

where $\langle \mathbf{X},Y \rangle = \frac{1}{T}\int_0^T (\mathbf{X}^* \cdot \mathbf{Y})dt$, $T = 2\pi/\omega$, and X^* is the complex conjugate of X. Evaluating Eq. (A36) leads to the amplitude equation

$$\partial_\tau A = \frac{1}{2\omega^2}\left(d - i\frac{2c}{\omega}\right)\Delta I_{e1}A$$
$$+ \frac{1}{2\omega^2}\left[cd - i\frac{1}{3\omega}(10c^2 + d^2\omega^2)\right]|A|^2A. \qquad (A37)$$

Near the Hopf bifurcation the original firing rates are given by Eq. (21).

Because the product cd is always positive, the real part of the cubic coefficient is also always positive, indicating that the Hopf bifurcation is *always* backward in the vicinity of the Takens-Bogdanov bifurcation. This immediately implies that there is no stable oscillatory solution (locally) since it can be shown that this unstable limit cycle disappears via a homoclinic bifurcation (as shown illustratively in Fig. 3); see [24] for details. This means that, there being no stable dynamical structures in the vicinity of the TB, the system is ejected locally.

4. LIF network

The equations are

$$\tau_A\frac{\partial P_A}{\partial t} = \frac{\sigma_A}{2}\frac{\partial^2 P_A}{\partial V_A^2} + \frac{\partial}{\partial V_A}\left[(V_A - I_{rec}^A(t) - I_{ext}^A)P_A\right], \qquad (A38)$$

together with the boundary conditions

$$P_A(V_t) = 0, \quad [P_A]_{V_r^-}^{V_r^+} = 0,$$

$$\frac{\partial P_A}{\partial V_A}(V_t) = -\frac{2\tau_A \nu_A(t)}{\sigma_A^2},$$

$$\left[\frac{\partial P_A}{\partial V_A}\right]_{V_r^-}^{V_r^+} = -\frac{2\tau_A \nu_A(t)}{\sigma_A^2}, \tag{A39}$$

where $[f]_{x_-}^{x_+} = \lim_{\epsilon \to 0}[f(x+\epsilon) - f(x-\epsilon)]$, as well as with the normalization $\int_{-\infty}^{V_t} dV_A P_A(V_A) = 1$. Here $\nu_A(t)$ is the time-varying firing rate of population A. This partial differential equation is coupled to the following different equations for the synaptic kinetics through the recurrent input

$$\tau_A^d \frac{ds_A}{dt} = -s_A + x_A,$$

$$\tau_A^r \frac{dx_A}{dt} = -x_A + \nu_A(t - \tau_l^A), \tag{A40}$$

where $\nu_A(t)$ is the firing rate of population A. Our goal is to study the oscillatory instabilities of the stationary state in these equations.

Stationary state and linear stability

The stationary state can be found to be

$$\nu_{A,0} = \frac{1}{\sqrt{\pi}\tau_A}\left[\int_{y_r^A}^{y_t^A} du\, e^{u^2}\mathrm{erfc}(-u)\right]^{-1}, \tag{A41}$$

where $y_t^A = \frac{V_t - I_{A,0}}{\sigma_A}$ and $I_{A,0} = I_{ext}^A + \tau_A(J_{AE}\nu_{E,0} - J_{AI}\nu_{I,0})$.

The linear stability of this solution is studied by expanding the dynamical variables as

$$\nu_A = \nu_{A,0} + \epsilon \nu_{A,1} e^{i\omega t}, \quad P_A = P_{A,0} + \epsilon P_{A,1} e^{i\omega t},$$

$$I_{rec}^A = I_{A,0} + \epsilon I_{A,1} e^{i\omega t}, \quad s_A = s_A^0 + \epsilon s_A^1 e^{i\omega t},$$

$$x_A = x_A^0 + \epsilon x_A^1 e^{i\omega t}, \tag{A42}$$

where $\epsilon \ll 1$. Additionally, we define the following variables:

$$Q_A = \frac{\sigma_A^2}{2\tau_A \nu_{A,0}}P_A, \quad y_A = \frac{V_A - I_{A,0}}{\sigma_A}. \tag{A43}$$

Then the linear stability problem can be expressed as

$$\frac{1}{2}Q_{A,1}'' + y_A Q_{A,1}' + (1 - i\omega\tau_A)Q_{A,1} = \frac{I_{A,1}}{\sigma_A}Q_{A,0}',$$

$$Q_{A,1}(y_t) = 0,$$

$$[Q_{A,1}]_{y_r^-}^{y_r^+} = 0, \tag{A44}$$

$$Q_{A,1}'(y_t) = -\frac{\nu_{A,1}}{\nu_{A,0}},$$

$$[Q_{A,1}']_{y_r^-}^{y_r^+} = -\frac{\nu_{A,1}}{\nu_{A,0}},$$

where, from the differential equations describing the synaptic kinetics we find that

$$I_{A,1} = \tau_A[J_{AE}R_E(\omega)e^{-i\Phi_E(\omega)}\nu_{E,1} - J_{AI}R_I(\omega)e^{-i\Phi_I(\omega)}\nu_{I,1}],$$

$$R_A(\omega) = \frac{1}{\sqrt{[1 + (\tau_A^d)^2\omega^2][1 + (\tau_A^r)^2\omega^2]}},$$

$$\Phi_A(\omega) = \tau_A^l\omega + \arctan(\tau_A^d\omega) + \arctan(\tau_A^r\omega). \tag{A45}$$

Solving for Eqs. (A44) yields the two-by-two system of linear equations

$$\begin{pmatrix} [U_E(i\omega)]_{y_r}^{y_t} - \frac{\tau_E J_{EE}\nu_{E,0}}{\sigma_E(1+i\tau_E\omega)}[U_E']_{y_r}^{y_t}A_E(\omega)e^{i\Phi_E(\omega)} & \frac{\tau_E J_{EI}\nu_{E,0}}{\sigma_E(1+i\tau_E\omega)}[U_E']_{y_r}^{y_t}A_I(\omega)e^{i\Phi_I(\omega)} \\ -\frac{\tau_I J_{IE}\nu_{I,0}}{\sigma_I(1+i\tau_I\omega)}[U_I'(i\omega)]_{y_r}^{y_t}A_E(\omega)e^{i\Phi_E(\omega)} & [U_I(i\omega)]_{y_r}^{y_t} + \frac{\tau_I J_{II}\nu_{I,0}}{\sigma_I(1+i\tau_I\omega)}[U_I']_{y_r}^{y_t}A_I(\omega)e^{i\Phi_I(\omega)} \end{pmatrix}\begin{pmatrix} \nu_{E,1} \\ \nu_{I,1} \end{pmatrix} = 0. \tag{A46}$$

Taking $J_{EE} = J_{IE} = J_E$ and $J_{II} = J_{EI} = J_I$ simplifies the determinant of Eq. (A46) considerably, leading to

$$1 + \frac{\tau_I J_I \nu_{I,0}}{\sigma_I(1 + i\tau_I\omega)}\frac{[U_I'(i\omega)]_{y_r}^{y_t}}{[U_I(i\omega)]_{y_r}^{y_t}}A_I(\omega)e^{i\Phi_I(\omega)} - \frac{\tau_E J_E \nu_{E,0}}{\sigma_E(1 + i\tau_E\omega)}\frac{[U_E'(i\omega)]_{y_r}^{y_t}}{[U_E(i\omega)]_{y_r}^{y_t}}A_E(\omega)e^{i\Phi_E(\omega)} = 0, \tag{A47}$$

where $U_A(y,\lambda) = \frac{e^{y^2}}{\Gamma(\frac{1+\lambda\tau_A}{2})}M(\frac{1-\lambda\tau_A}{2}, \frac{1}{2}, -y^2) + \frac{2ye^{y^2}}{\Gamma(\frac{\lambda\tau_A}{2})}M(1 - \frac{\lambda\tau_A}{2}, \frac{3}{2}, -y^2)$ and $M(a,b,z)$ is the confluent hypergeometric function; see [37].

Zeros of this complex equation give the combination of parameters for which an oscillatory instability occurs with frequency ω. When $\omega = 0$ this equation takes the particularly simple form

$$1 + \tau_I J_I \frac{\partial \nu_{I,0}}{\partial I_{I,0}} - \tau_E J_E \frac{\partial \nu_{E,0}}{\partial I_{E,0}} = 0, \tag{A48}$$

where $\frac{\partial \nu_{A,0}}{\partial I_{A,0}} = \frac{\sqrt{\pi}\tau_A \nu_{A,0}^2}{\sigma_A}[e^{y^2}\mathrm{erfc}(-y)]_{y_r}^{y_t}$. Equation (A47) can be hard to solve because one needs to evaluate confluent hypergeometric functions for which there is no general scheme. An alternative approach is to solve the PDE via Laplace transforms, which leads to a stability criterion in terms of integrals, which are easier to evaluate.

Stationary state and linear stability via Laplace Transform

This method of solution is described in detail in [38]. The Fokker-Planck equation, Eq. (A38) can be written

$$\frac{\partial P_A}{\partial t} + \frac{\partial F_A}{\partial \nu_A} = \nu_A[\delta(V_A - V_r) - \delta(V_A - V_t)],$$

$$F_A = -\frac{\sigma_A^2}{2\tau_A}\frac{\partial P_A}{\partial V_A} - \frac{V_A - I_A}{\tau_A} P_A, \quad (A49)$$

where $F_A(V_A)$ is the probability flux, I_A is the total current, and the reset condition has now been incorporated directly into the PDE. Once again we perform the expansion Eqs. (A42) (the ODEs describing the synaptic activity are solved as before and so are not explicitly shown here). We additionally expand $J_A = J_{A,0} + \epsilon J_{A,1}e^{i\omega t}$.

The order one equations are

$$\frac{dF_{A,0}}{dV_A} = \nu_{A,0}[\delta(V_A - V_r) - \delta(V_A - V_t)],$$

$$F_{A,0} = -\frac{\sigma_A^2}{2\tau_A}\frac{dP_{A,0}}{dV_A} - \frac{V_A - I_{A,0}}{\tau_A} P_{A,0}. \quad (A50)$$

These equations are transformed using a generalized Laplace transform; see [38]. This leads to an equation for the transformed probability density,

$$\frac{d\tilde{P}_{A,0}}{ds} - \left(I_{A,0} + s\frac{\sigma_A^2}{2}\right)\tilde{P}_{A,0} = \frac{\tau_A \nu_{A,0}}{s}(e^{sV_r} - e^{sV_t}), \quad (A51)$$

where $\tilde{f}(s) = \int_{-\infty}^{\infty} dv e^{vs} f(v)$. Solving this first order ODE and then imposing the condition $\tilde{P}(0) = 1$, yields

$$\nu_{A,0} = \frac{1}{\tau_A}\left[\int_0^\infty \frac{dy}{y}e^{-y^2}\left(e^{2yy_t^A} - e^{2yy_r^A}\right)\right]^{-1}, \quad (A52)$$

which shows the equivalence of the integrals in Eqs. (A41) and (A52).

At order ϵ the equations are

$$i\omega P_{A,1} + \frac{dF_{A,1}}{dV_A} = \nu_{A,1}[\delta(V_A - V_r) - \delta(V_A - V_t)],$$

$$F_{A,1} = -\frac{\sigma_A^2}{2\tau_A}\frac{dP_{A,1}}{dV_A} - \frac{V_A - I_{A,0}}{\tau_A}P_{A,1} + \frac{I_{A,1}}{\tau_A}P_{A,0}, \quad (A53)$$

which, once transformed, give

$$\frac{d\tilde{P}_{A,1}}{ds} - \left(I_{A,0} + s\frac{\sigma_A^2}{2} - \frac{i\tau_A\omega}{s}\right)\tilde{P}_{A,1}$$

$$= I_{A,1}\tilde{P}_{A,0} + \frac{\tau_A \nu_{A,1}}{s}(e^{sV_r} - e^{sV_t}). \quad (A54)$$

Solving this equation and imposing the condition that $\tilde{P}_{A,1}(0) = 0$ gives

$$\nu_{A,1} = \frac{2I_{A,1}\nu_{A,0}}{\sigma_A(1 + i\tau_A\omega)}\frac{B_A^1(\omega)}{B_A^0(\omega)}, \quad (A55)$$

where $B_A^n(\omega) = \int_0^\infty \frac{dy}{y}y^n e^{-y^2}(e^{2yy_t^A} - e^{2yy_r^A})y^{i\tau_A\omega}$. The conditions for the two populations A are coupled through the currents $I_A = \tau_A J_{AE}\nu_E A_E(\omega)e^{i\Phi_E(\omega)} - \tau_A J_{AI}\nu_I A_I(\omega)e^{i\Phi_I(\omega)}$, which leads again to a system of two coupled linear equations. Setting the determinant equal to zero (with $J_{EE} = J_{IE} = J_E$ and $J_{II} = J_{EI} = J_I$) yields

$$1 + \frac{\tau_I J_I \nu_{I,0}}{\sigma_I(1 + i\tau_I\omega)}2\frac{B_I^1(\omega)}{B_I^0(\omega)}A_I(\omega)e^{i\Phi_I(\omega)}$$

$$- \frac{\tau_E J_E \nu_{E,0}}{\sigma_E(1 + i\tau_E\omega)}2\frac{B_E^1(\omega)}{B_E^0(\omega)}A_E(\omega)e^{i\Phi_E(\omega)} = 0, \quad (A56)$$

which, comparing with Eq. (A47) shows that $\frac{[U_A'(i\omega)]_{y_r}^{y_t}}{[U_A(i\omega)]_{y_r}^{y_t}} = 2\frac{B_A^1(\omega)}{B_A^0(\omega)}$. The advantage of the Laplace transform method is the ease with which the integrals can be evaluated.

When $\omega = 0$ note that it can easily be shown that $B_A^0(0) = \frac{1}{\tau_A \nu_{A,0}}$ and $B_A^1(0) = \frac{\sqrt{\pi}}{2}[e^{y^2}\text{erfc}(-y)]_{y_r^A}^{y_t^A}$, which agrees with (A48).

Stability of slow oscillations

Another advantage of the Laplace transform method is that the resulting integrals can be easily expanded for small ω. This is the relevant expansion near the Takens-Bogdanov codimension-two point where the oscillations go to zero. In this case we have

$$B_A^n(i\omega) \sim B_A^n(0) + \left.\frac{\partial B_A^n}{\partial(i\omega)}\right|_{\omega=0}i\omega - \left.\frac{\partial^2 B_A^n}{\partial(i\omega)^2}\right|_{\omega=0}\omega^2,$$

$$= \frac{1}{\tau_A \nu_{A,0}} + b_A^{n,1}i\tau_A\omega - b_A^{n,2}\tau_A\omega^2, \quad (A57)$$

where

$$b_A^{n,k} = \int_0^\infty dy y^{n-1}[\ln y]^k e^{-y^2}(e^{2yy_{A,t}} - e^{2yy_{A,r}}). \quad (A58)$$

---

[1] H. R. Wilson and J. D. Cowan, Biophys. J. **12**, 1 (1972).

[2] H. R. Wilson and J. D. Cowan, Kybernetik **13**, 55 (1973).

[3] N. Brunel, J. Comput. Neurosci. **8**, 183 (2000).

[4] G. B. Ermentrout and J. D. Cowan, J. Math. Biol. **7**, 265 (1979).

[5] N. Brunel and X.-J. Wang, J. Neurophysiol. **90**, 415 (2003).

[6] N. Brunel and V. Hakim, Neural Comp. **11**, 1621 (1999).

[7] A. Gevins, M. E. Smith, L. McEvoy, and D. Yu, Cereb. Cortex **7**, 374 (1997).

[8] C. D. Tesche and J. Karhu, Proc. Natl. Acad. Sci. USA **97**, 919 (2000).

[9] S. Raghavachari, M. J. Kahana, D. S. Rizzuto, J. B. Caplan, M. P. Kirschen, B. Bourgeois, J. R. Madsen, and J. E. Lisman, J. Neurosci. **21**, 3175 (2001).

[10] H. Lee, G. V. Simpson, N. K. Logothetis, and G. Rainer, Neuron **45**, 147 (2005).

[11] D. Jokisch and O. Jensen, J. Neurosci. **27**, 3244 (2007).

[12] B. Spitzer, E. Wacker, and F. Blankenburg, J. Neurosci. **30**, 4496 (2010).

[13] K. Wimmer, M. Ramon, T. Pasternak, and A. Compte, J. Neurosci. **36**, 489 (2015).

[14] C. Tallon-Baudry, O. Bertrand, F. Peronnet, and J. Pernier, J. Neurosci. **18**, 4244 (1998).

[15] B. Pesaran, J. S. Pezaris, M. Sahani, P. P. Mitra, and R. A. Andersen, Nat. Neurosci. **5**, 805 (2002).

[16] M. W. Howard, D. S. Rizzuto, J. B. Caplan, J. R. Madsen, J. Lisman, R. Aschenbrenner-Scheibe, A. Schulze-Bonhage, and M. J. Kahana, Cereb. Cortex **13**, 1369 (2003).

[17] J. Fell and N. Axmacher, Nat. Rev. Neurosci. **12**, 105 (2011).

[18] G. B. Ermentrout, Neural Comput. **6**, 679 (1994).

[19] O. Shriki, D. Hansel, and H. Sompolinsky, Neural Comput. **15**, 1809 (2003).

[20] E. Montbrió, D. Pazó, and A. Roxin, Phys. Rev. X **5**, 021028 (2015).

[21] D. Hansel and C. van Vreeswijk, J. Neurosci. **22**, 5118 (2002).

[22] E. K. Miller and T. W. Troyer, J. Neurophysiol. **87**, 653 (2002).

[23] A. Roxin, Front. Comput. Neurosci. **5:8**, 1 (2011).

[24] S. Wiggins, *Introduction to Applied Nonlinear Dynamical Systems and Chaos*, 2nd ed. (Springer, Berlin, 2003).

[25] E. Ledoux and N. Brunel, Front. Comp. Neurosci. **5**, 25 (2011).

[26] G. Buzsáki and A. Draguhn, Science **304**, 1926 (2004).

[27] N. Brunel and V. Hakim, Chaos **18**, 015113 (2008).

[28] C. Geisler, N. Brunel, and X.-J. Wang, J. Neurophysiol. **94**, 4344 (2005).

[29] B. K. Murphy and K. D. Miller, Neuron **61**, 635 (2009).

[30] D. B. Rubin, S. D. V. Hooser, and K. D. Miller, Neuron **85**, 402 (2015).

[31] A. Roxin, N. Brunel, and D. Hansel, Phys. Rev. Lett. **94**, 238103 (2005).

[32] A. Roxin and D. Montbrió, Phys. D (Amsterdam, Neth.) **240**, 323 (2011).

[33] E. S. Schaffer, S. Ostojic, and L. F. Abbott, PLoS Comp. Biol. **9**, e1003301 (2013).

[34] R. M. Borisyuk and A. B. Kirillov, Biol. Cybern. **66**, 319 (1992).

[35] A. Compte, N. Brunel, P. S. Goldman-Rakic, and X.-J. Wang, Cereb. Cortex **10**, 910 (2000).

[36] J. P. Ramírez-Mahaluf, A. Roxin, H. S. Mayberg, and A. Compte, Cereb. Cortex (2015), doi:10.1093/cercor/bhv249.

[37] N. Brunel and D. Hansel, Neural Comput. **18**, 1066 (2006).

[38] M. J. E. Richardson, Phys. Rev. E **76**, 021919 (2007).